UNIVERSITY OF OKLAHOMA

GRADUATE COLLEGE

WETTABILITY ALTERATION USING FLUORINATED NANO-SILICA FOR NEAR WELLBORE REGION

A THESIS

SUBMITTED TO THE GRADUATE FACULTY

in partial fulfillment of the requirements for the

Degree of

MASTER OF SCIENCE

By

SHASHWAT AGARWAL
Norman, Oklahoma
2016

Downloaded from SHAREOK. Persistent Handle URL: https://hdl.handle.net/11244/47104

WETTABILITY ALTERATION USING FLUORINATED NANO-SILICA FOR NEAR WELLBORE REGION

A THESIS APPROVED FOR THE
MEWBOURNE SCHOOL OF PETROLEUM AND GEOLOGICAL ENGINEERING

BY

_____
Dr. Mashhad Fahs, Chair

_____
Dr. Maysam Pournik

_____
Dr. Catalin Teodoriu

© Copyright by SHASHWAT AGARWAL 2016
All rights Reserved.

Acknowledgements

First, I would like to thank Dr.Fahs, for being such a terrific advisor. Without her guidance and support, this would not have been possible. I also want to thank Dr.Catalin for helping me with building equipment in the lab and Dr.Pournik for providing help in starting out this work.

Next, I want to thank Joe and Garry, the lab techs who helped me setup the lab and equipment. I am also very grateful to the MPGE department for their support.

Finally, friends and family. Your constant encouragement saw me through. Jocin, Israel, Mehana you guys helped whenever I needed it. Mom, I know it was hard not seeing me for years, but we made it. Dad you'll always be missed.

Table of Contents

Acknowledgements iv

Table of Contents v

List of Figures vii

List of Tables x

Abstract xi

Introduction 1

Literature Review 4

Wettability modifiers 4

Theoretical background 9

Wettability and Contact Angles 9

Spontaneous Imbibition 11

Relative Permeability 12

Porosity 13

Permeability 14

Treatment Mechanism 20

Proppant pack flooding 23

Experiment Design and Methodology 24

Contact angle measurement 24

Preparation of core samples 26

Porosity meter 26

Imbibition setup 29
Permeability measurement 33
Treatment design 35
Proppant pack flooding 38
Simulation setup 43
Results and Discussions 48
Wettability alteration, contact angle results 48
Wettability Alteration, permeability results 50
Wettability Alteration, imbibition results 54
Proppant Pack Flooding, Permeability, and Relative permeability 59
Simulation results 68
Cost Analysis 68
Scope for continued research 69
References 71

List of Figures

Figure 1: Liquid droplet through pores, untreated and treated surfaces. 2

Figure 2: Condensate and water build-up in gas condensate reservoirs. 2

Figure 3: Comparison of pre/post treatment production rates for a gas well 5

Figure 4: A picture and a schematic to demonstrate contact angles. 9

Figure 5: Contact angle measurement using DSA.. 10

Figure 6: Spontaneous imbibition results for three rocks, plotted as recovery fraction. 11

Figure 7: Typical Relative Permeability curves for two-phase flow 12

Figure 8: Gas Darcy Law plot for 3 rock samples 16

Figure 9: Darcy plot for non-Darcy flow through a proppant pack 16

Figure 10: Forchheimer Plot for three different proppant packs 17

Figure 11: Molecular structure of TEOS and PFDS 21

Figure 12: Chemical reaction between PFDS and TEOS 21

Figure 13: Schematic of rock substrate treated with PFDS and TEOS 22

Figure 14: Contact angle measurement setup 25

Figure 15: Porosity meter 27

Figure 16: Sample porosity calculation from MS Excel 29

Figure 17: Sample Calculation for imbibition recovery fraction. 30

Figure 18: Imbibition setup 31

Figure 19: Setup to measure gas permeability. 33

Figure 20: Picture of Hassler type core-holder on a stand 33

Figure 21: Sample Permeability Calculations 35

Figure 22: Core flooding/treatment setup 37

Figure 23: Proppant pack, 40x70 Sand 38

Figure 24: Sand pack setup schematic 39

Figure 25: Sand pack picture 1 39
Figure 26: Sand pack picture 2. 40
Figure 27: Relative permeability calculations, 1 42
Figure 28: Relative permeability calculations, 2 42
Figure 29: Relative permeability calculations, 3 43
Figure 30: Reservoir and fracture represented in CMG 45
Figure 31: Relative permeability for Case 1 (Sand in fracture zone) 45
Figure 32: Relative Permeability for Case 2 (Resin Coated Sand in Fracture) 46
Figure 33: Relative Permeability contrast between Sand and RCS 47
Figure 34: Untreated glass slide, water-air contact angle. 48
Figure 35: Water and Oil droplets on a glass slide with Treatment A (PFDS-1). 48
Figure 36: Water and Oil droplets on a glass slide with Treatment B (PFDS-2). 49
Figure 37: GB1 and GB2 treated with PFDS-1 and PFDS-2 respectively. 49
Figure 38: GB1 and GB2 treated with PFDS-1 and PFDS-2 respectively. 50
Figure 39: Permeability contrast, before and after treatment, PFDS-1 50
Figure 40: Polymer residue on a glass slide treated with PFDS-1 51
Figure 41: Permeability contrast, before and after treatment, PFDS-2 52
Figure 42: LS1 Permeability test results with PFDS-2 treatment. 52
Figure 43: LS3 permeability contrast with PFDS-2 treatment. 53
Figure 44: Imbibition in reference rocks (untreated rocks) 54
Figure 45: Hysteresis effect of imbibition in different samples (untreated) 55
Figure 46: Air bubbles sticking to rock surface during water imbibition. 55
Figure 47: Water and Decane imbibition in Limestone 56
Figure 48: Water and Decane imbibition in Sandstone 57
Figure 49: Relative Permeability curves for oil-water, 40x70 Sand 59
Figure 50: Relative Permeability curves for oil-water, 50x80 RCS 61

Figure 51: Relative permeability comparison between RCS and Sand..... 62

Figure 52: Non-Darcy relative permeability for RCS. 63

Figure 53: Non-Darcy relative permeability for Sand. 64

Figure 54: Non-Darcy Forchheimer equation between 50cc/min and 100cc/min flowrates for Oil and Water in Sand. 65

Figure 55: Non-Darcy Forchheimer equation between 50cc/min and 100cc/min flowrates for Oil and Water in RCS. 66

Figure 56: Simulated water production rates..... 69

List of Tables

Table 1: Contact angle sample calculation. 26

Table 2: Rock samples (untreated and treated) information 26

Table 3: Treatment chemicals 35

Table 4: Chemical ratios for Treatments A & B. 36

Table 5: Reservoir properties for simulator 44

Table 6: Relative permeability tables for reservoir rock 46

Table 7: Relative permeability tables for the fracture zone 47

Table 8: Relative permeability table for Oil-water system in Sand. 60

Table 9: Relative permeability table for Oil-water ssytem in RCS 61

Table 10: Non-Darcy relative permeability table for RCS. 63

Table 11: Non-Darcy relative permeability table for Sand 64

Table 12: Sand relative permeability data, Forchheimer calculations 66

Table 13: RCS relative permeability data, Forchheimer calculations 67

Table 14: Simulation run summary 68

Table 15: Cost Analysis for treatment 69

Abstract

Fluorinated nano-Silica particles are capable of coating silica and limestone substrates with an amphiphobic layer. A layer that repels both water and oil to some extent. The polymer formed with PFDS and TEOS is capable of forming strong permanent bonds with silica substrates. This imparts the treatment exceptional durability and stability. The effect of this treatment on permeability and porosity was studied. Contact angle study, high temperature stability and impact on permeability were the elimination criterion for selecting a possible candidate treatment candidate. With the help of the Sol-gel Stober process, suspended fluorinated organic monomers were generated, which polymerized to form the treatment chemical. Finally, a simulation study helped verify the perks theorized for field scale application of this treatment.

Introduction

In gas condensate reservoirs, liquid saturation starts dropping out from gas phase as the flowing bottom hole pressure drops below the dew point pressure of reservoir fluid. Due to the presence of capillary forces, this liquid can remain trapped. This phenomenon is referred to as "condensate banking" and it can severely impact production from a well. For example, a productivity loss of 50% in the Arun field has been attributed to liquid dropout of 1.1% from reservoir fluid (Afidick, Kaczorowski, & Bette, 1994).

A significant number of experimental as well as theoretical studies have been conducted to understand, model and predict condensate behavior and its impact on well productivity (Fahimpour, Jamiolahmady, Severac, & Sohrabi, 2012). Historically, several practical methods to prevent, delay or treat this problem have been implemented with varying degree of success.

Hydraulic fracturing has been a popular choice to mitigate condensate banking and to restore well productivity in gas/condensate reservoirs. Horizontal and deviated wells exhibit a lower pressure drawdown and milder liquid blockage effects near the wellbore region (Dehane & Tiab, 2000). Dry-gas recycling in Sleipner field resulted in restoration of reservoir pressure and an increased condensate recovery of 25% (Eikeland & Hansen, 2009). Solvent injection has also been employed for treating condensate banking near the wellbore region. Methanol injection in Hatters Pond gas field resulted in twofold increase in the productivity of wells for the initial 4 months after solvent injection (Du, Walker, Pope, Sharma, & Wang, 2000). These methods though successful, have an inherent problem. They are a temporary fix, and over the life of a well, several such treatments could be required to maintain well productivity.

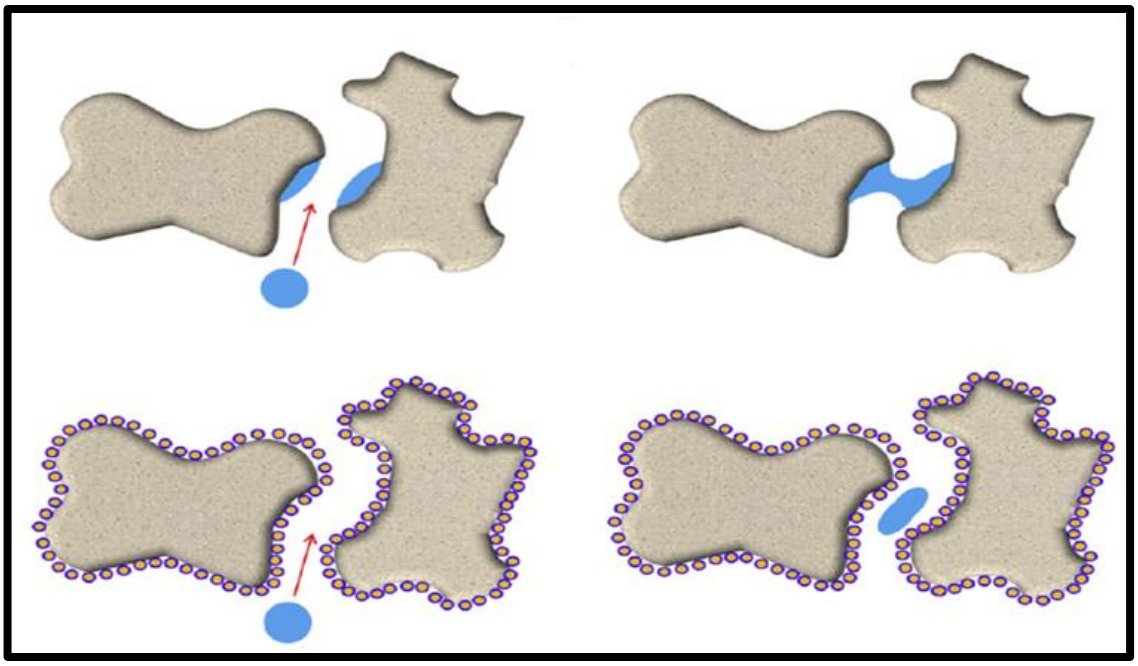


Figure 1: Liquid droplet through pores, untreated and treated surfaces. (Mousavi, Hassanajili, & Rahimpour, 2013)

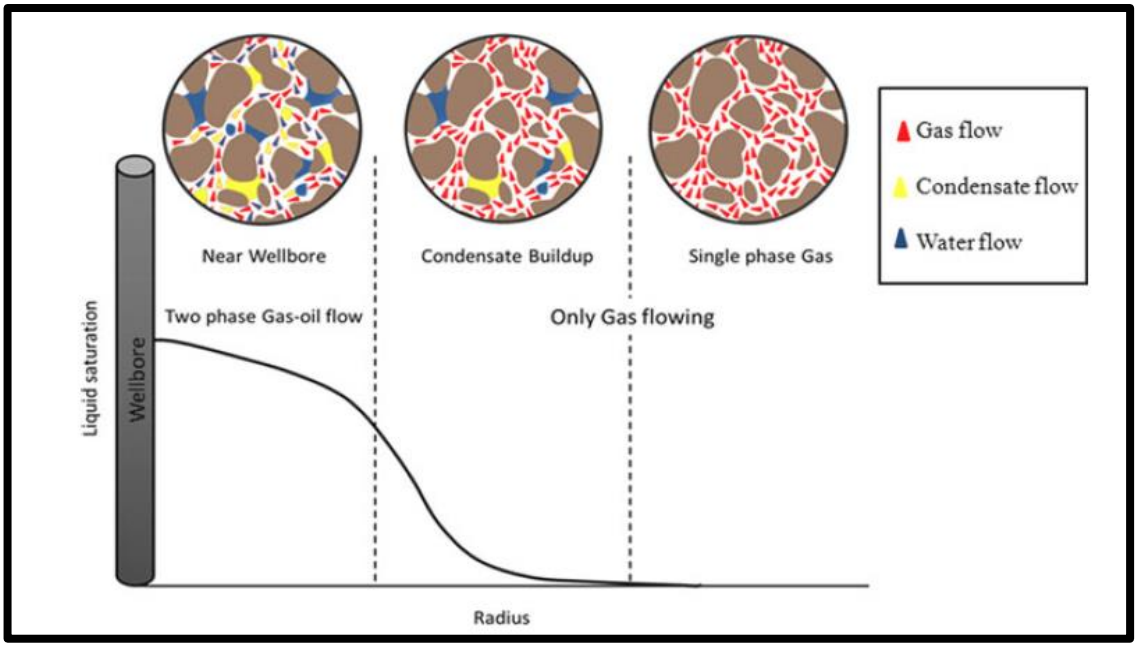


Figure 2: Condensate and water build-up in gas condensate reservoirs. (Sharifzadeh et al., 2013)

Firoozabadi (Li & Firoozabadi, 2000) conducted tests by altering the wettability of reservoir rock near the wellbore region to improve mobility of dropped out condensate. This led to another avenue being opened for treating the problem of condensate banking.

Since then several researchers have tried to address condensate banking with wettability modifiers. The reason this method is getting significant attention is because it can be a permanent fix for the near wellbore region.

This work deals with altering the wettability of silica and limestone substrates using a nano-coating of fluorinated silica to enhance liquid mobility. The effects of this treatment on porosity, permeability and possible application to proppant packs were studied. To demonstrate the intermediate wet properties of treated cores, contact angle measurements and spontaneous imbibition experiments were conducted.

Literature Review

Wettability modifiers

Wettability modifiers are chemicals capable of altering the wettability characteristics of rock surfaces. Presented in this work, next is a review of current work done with wettability modifiers.

(Li & Firoozabadi, 2000) performed wettability alteration of rocks to preferential gas-wetting by using fluoro-polymers FC754 and FC722. It was demonstrated with the use of FC754 that the contact angles in a glass capillary tube were altered from 50 to 90^{o} for a water-air system and 0 to 60^{o} for a decane-air system. The results were qualitatively better when FC722 was employed, with contact angles varying from 50 to 120^{o} and 0 to 60^{o} for water air and decane-air systems respectively. Additionally, imbibition experiments were conducted to demonstrate the efficiency of the suggested treatment. It was concluded that altering the wettability of rocks could improve effective gas permeability because it prevents liquid accumulation in high saturations near the wellbore region. This work was a proof of concept, which successfully demonstrated the possibility of further research.

(Tang & Firoozabadi, 2002) further continued previous work and performed wettability alteration for temperatures as high as 90^{o}C. Results reported include successful wettability alteration, durability of treatment (FC759) and the effect of this treatment on relative permeabilities for gas and oil.

(Adibhatla, Mohanty, Berger, & Lee, 2006) investigated several surfactants for their performance in mitigating water buildup near fracture and wellbore region in tight-gas wells. Set of experiments were conducted with Fluorosilanes, cationic and anionic

amines, fluorinated surfactants, and polymers. Fluorosilanes demonstrated good water repellency on calcite and mica. The amines became unstable with addition of field brine thus, they were discarded. The fluorinated surfactants and polymers formed gels and suspensions with addition of field brine, which adversely affected their ability to be adsorbed on rock surfaces. Fluorosilanes demonstrated promising results and good stability with fields conditions. Further study was recommended for their most successful chemicals (1H,1H,2H,2Hperfluorodecyltriethoxysilane and FloroPel) and it was concluded that fluorinated polymers are the best bet towards field scale wettability alteration of reservoir rocks.

(Panga et al., 2006) analyzed five different fluoropolymers. The study reported that four of the five tested chemicals were unfeasible at reservoir conditions, while the fifth chemical was stable and provided good results, but it resulted in permeability reduction of 50%.

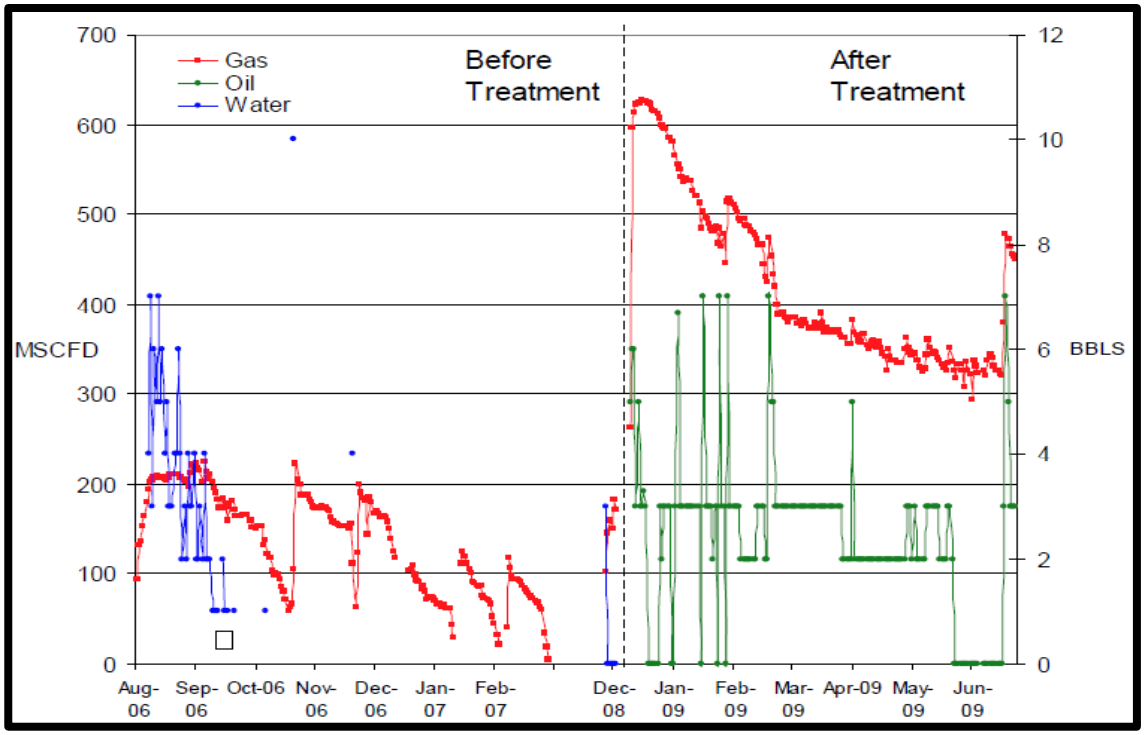


Figure 3: Comparison of pre/post treatment production rates for a gas well (Butler et al., 2009)

(Kumar, Pope, & Sharma, 2006) were able to successfully treat sandstone cores with a non-ionic surfactant carried in methanol-water solution for temperatures ranging from 145^{o}F to 275^{o}F. This treatment improved condensate relative permeability by a factor of 2. The chemicals tested had fluorochemical group to provide oil and water repellant properties, and either silanol or alkoxy group to provide bonding to rock surface. The treatment though did not produce feasible results for carbonate cores and was unstable with salts. (Bang, Pope, Sharma, Baran, & Ahmadi, 2008), were able to overcome this by replacing the methanol-water mixture with glycol-alcohol mixture. (Butler et al., 2009), conducted field scale application of this treatment in Lower Morrow Sandstone reservoir in Oklahoma. The reservoir gas production increased by 300% for the 7-month study period after treatment. (Ahmadi et al., 2011), extended this work further by successfully treating carbonate rocks. The authors achieved this by using an amine primer, which improved adsorption of this chemical on carbonate surface.

(Fahes & Firoozabadi, 2007), started the work with an initial focus on testing treatments for intermediate gas wetting at 140^{o}C. It was observed that FC759 and FC722 are ineffective at reservoir conditions. Effects of 10 different chemicals were examined and several of those failed initial screening tests (ineffective at reservoir conditions and desorption from rock substrate at higher temperatures). Low molecular weight monomers 11-12P and L-18941 from 3M were later synthesized and selected for further study. Results of treatment of rock samples with different concentrations of 11-12P and L-18941 were promising. Some concentrations exhibited increased liquid mobility, permanent treatment, and no reduction in absolute permeability of rocks. 3M halted the production of these chemicals due to environmental concerns.

(Wu & Firoozabadi, 2010), investigated the effect of salts on wettability altering treatments. It was reported that the salts generally present in drilling muds, fracturing fluids and interstitial water severely impacted effectiveness of the treatment. The authors demonstrated that while salts had a huge detrimental effect on treatment performance, pre-treatment by displacing interstitial fluids with water, followed by nitrogen possibly neutralized the effect of residual salts.

(Mousavi et al., 2013), attempted developing an effective method of modifying wettability of the reservoir rock. The authors reported successful synthesis of fluorinated nano-silica particles by co-hydrolysis of Tetraethylorthosilicate (TEOS) and a fluorinated alkylsilane (FAS) in ethanol and ammonium hydroxide solution. This was an adoption of the Stober process to generate silica nanoparticles. SEM images of treated cores were obtained to confirm the presence of functionalized nano-silica particles on rock surface. The study dealt more with creation and coating of silica-nano particles on rock surface, rather than petrological aspects of the treatment. EDX analysis of cross-sections of treated cores was employed to confirm the successful transport of silica nano-particles dispersed in ethanol throughout the core. The contact angle results obtained were in-line with previous experiments by author's peers (S. Sharifzadeh, Sh. Hassanajili and M.R. Rahimpour).

(Sharifzadeh et al., 2013) proposed utilization of the sol-gel process for development of an effective coating film on rock substrate resulting in wettability alteration. The authors experimented with Triethoxy-1H,1H,2H,2Hperfluorodecylsilane (PFDS) on limestone surface. Fourier transform infrared (FTIR) spectroscopy, scanning electron microscopy (SEM) and electron dispersive analysis of X-ray (EDX) were conducted to characterize

the treatment properties. Static contact angle measurements and imbibition tests to determine the efficiency of wettability alteration were also performed. Limestone samples from Sarkhum reservoir, NaCl brine and normal decane were the basic materials employed by this team to study efficiency of the proposed treatment. The primary objective, to examine the covalent molecular bond formation with limestone surface. FTIR and SEM-EDX tests confirmed hydrophobic and oleophobic characteristics of the coating film, thus confirming success of sol-gel reactions. Additionally, SEM-EDX confirmed sol-gel bonding between mineral grains (hydroxyl groups) and PFDS. Contact angle and imbibition tests confirmed the successful wettability alteration of samples treated with PFDS and TEOS solution. The authors concluded, that gas permeability was increased due to improved liquid mobility and the PFDS+TEOS solution could be an effective tool to protect the Sarkhum reservoir from condensate damage.

(Fahimpour et al., 2012) started the work with a screening procedure for testing chemicals, followed by extensive tests with selected chemicals on carbonate outcrop samples. They concluded that anionic and nonionic chemicals were the most effective while cationic and amphoteric chemicals were the worst. To minimize the effect of salts on chemicals, an alcohol based solvent was effective. Combined with a filtration system, their chemicals could successfully treat the rocks, without damaging absolute permeability. Additionally, the initial screening procedure employed by the authors was effective in selecting chemicals that were expected to perform well.

Theoretical background

Wettability and Contact Angles

Wettability is defined as the tendency of one fluid to spread or to adhere to a solid surface in the presence of other immiscible fluids (Craig, 1993). It's a microscopic characteristic, requiring micro-scale laboratory investigation techniques for measurement. The evaluation of reservoir wettability is possible through measurements of interfacial tension and contact angles. Contact angle, θ is conventionally, the angle where a liquid-vapor interface meets a solid surface. In petroleum engineering, oil-water/brine pairs are of interest. The angle θ, is influenced by the fluids. In presence of two immiscible fluids (e.g. water and oil), the fluid with tendency to spread on the surface of pore walls is the wettability preference of that rock type. The degree to which this preference is exhibited is controlled both by the chemical composition of fluids and properties of the pore wall i.e. properties of the rock. Asphaltene content of oil, salinity of water, surface roughness of pore wall and surface free energy are some of the factors that determine the wettability preference in a system. This work deals with changing the wettability of surfaces from

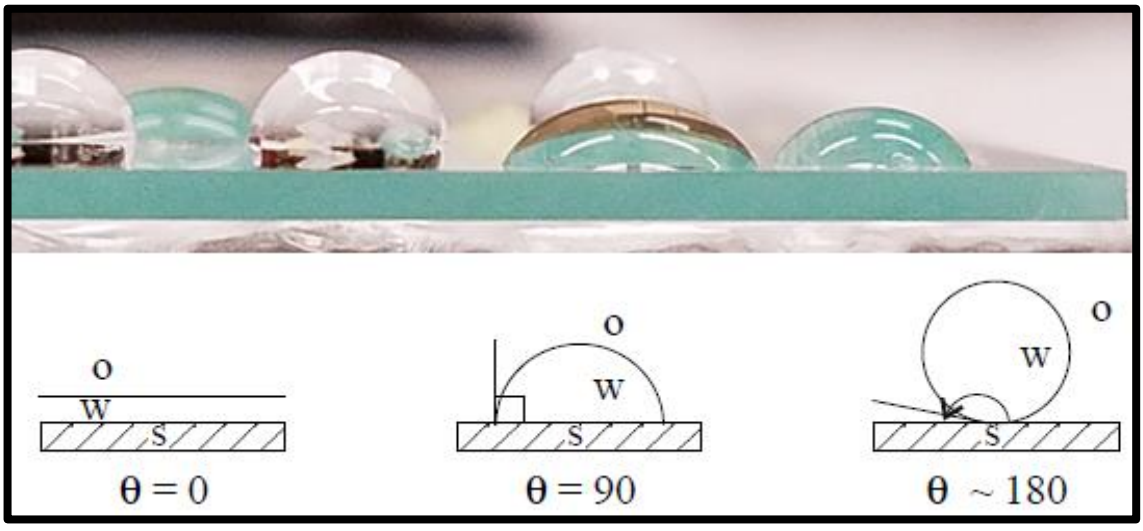


Figure 4: A picture and a schematic to demonstrate contact angles. In the picture, Water (left, contact angle of 102.6°) and Oil (right, contact angle of 57.5°) droplets on a treated glass slide. Schematic, O = Oil, W = Water, S = Solid surface.

strongly water wet to intermediate wet. An intermediate wet surface would exhibit contact angles in the range of 70°-120° for water-air interface, 20°-60° for oil-air interface. Oil in this work refers to N-decane, NC10. Several methods for measuring contact angles exist. The most popular being sessile drop method, which measures contact angle with the help of a goniometer. Another popular method is drop shape analysis (DSA). The DSA method captures an image of a drop, and takes it to be a clipped part of a whole sphere. Thus, by measuring the width and height of a droplet, imagined to be part of a sphere, contact angle is calculated. Contact angle in radians by this method is calculated as –

$$\theta = 2.\arctan\left(\frac{2.H}{W}\right)$$

θ, is the contact angle (radians)

$arctan$, inverse trigonometric function of 'tangent', usually referred to as 'arctan'.

H, height of droplet from solid surface.

W, width of the droplet.

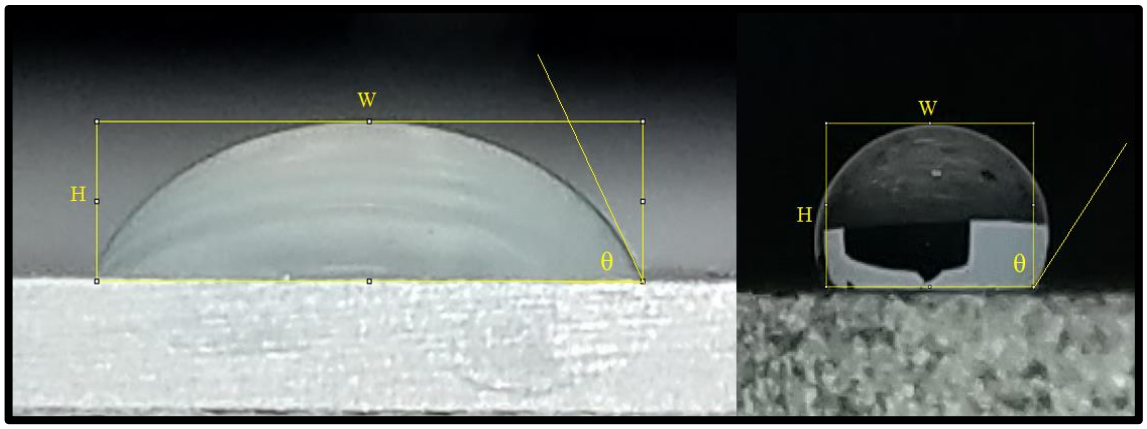


Figure 5: Contact angle measurement using DSA. Decane droplet on a treated glass slide (left). Water droplet on a treated core sample (right).

Spontaneous Imbibition

Spontaneous imbibition, a process which allows wetting fluid to be drawn inside a porous media by effect of capillary forces. It is driven by surface energy, under action of capillary pressure. Capillary pressure is a difference in pressure across an interface between two immiscible fluids.

Spontaneous Imbibition experiments can qualitatively categorize relative permeability characteristics of porous media. Thus, imbibition experiments in this work were conducted with the aim of testing effectiveness of wettability modifiers. To this end, numerous experiments were conducted with fresh, untreated, used and treated core

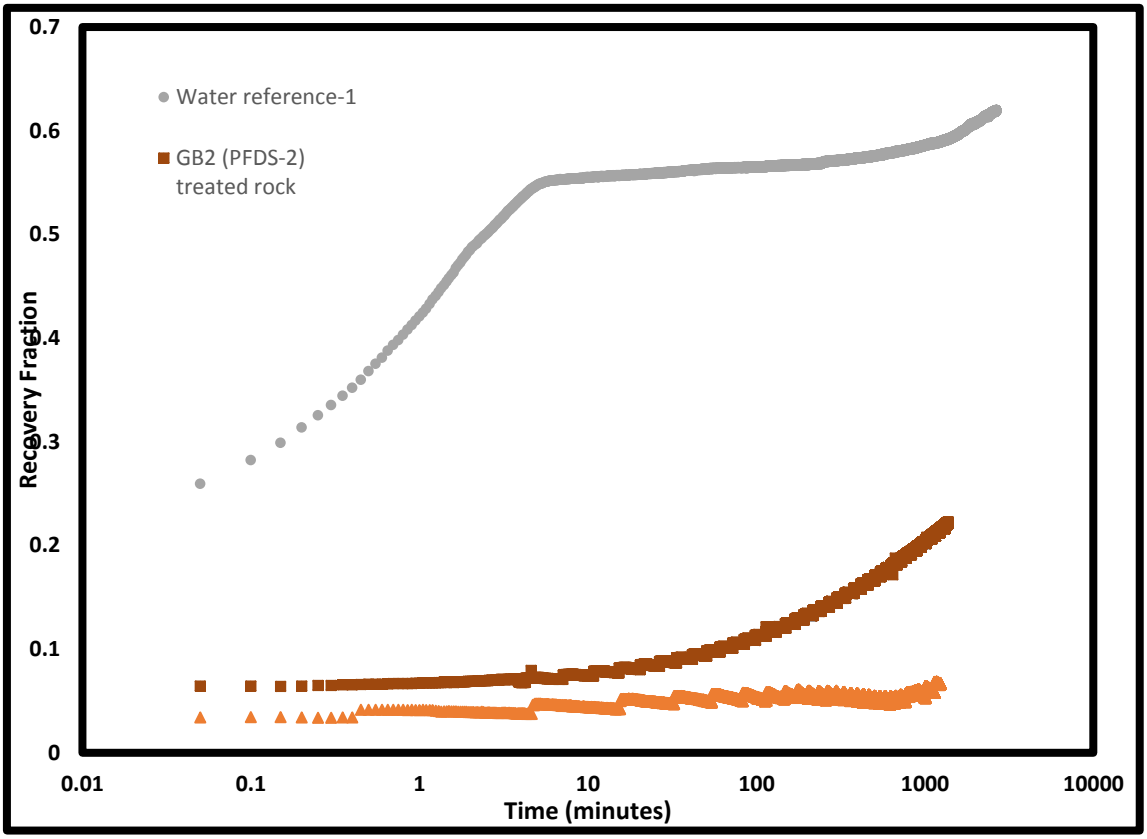


Figure 6: Spontaneous imbibition results for three rocks, plotted as recovery fraction.

samples. A rock with most desirable wettability characteristics would have a very low

recovery fraction. Since it would imply a lower capillary pressure for that fluid (oil or water). Ergo, lower recovery fractions are the better results.

Relative Permeability

It has been established, that wettability characteristics of a reservoir rock impact recovery. e.g. Water flooding studies cannot be done, without considering the wettability of rocks. Introduction section of this work, Figure 1 and Figure 2, depicted an example of rock wettability on oil recovery from reservoirs. Relative permeability tables are one of the tools available to study wettability characteristics of rocks with two-phase flow. Under two-phase flow, the phases are immiscible, e.g. Oil and water are two different phases, when referring relative permeability. Relative permeability is a concept that relates absolute permeability (permeability with a fluid at 100% saturation in the porous media) of a system, to the effective permeability of a fluid in that system, when the fluid occupies just a fraction of the total pore volume (Zolotukhin & Ursin, 1997).

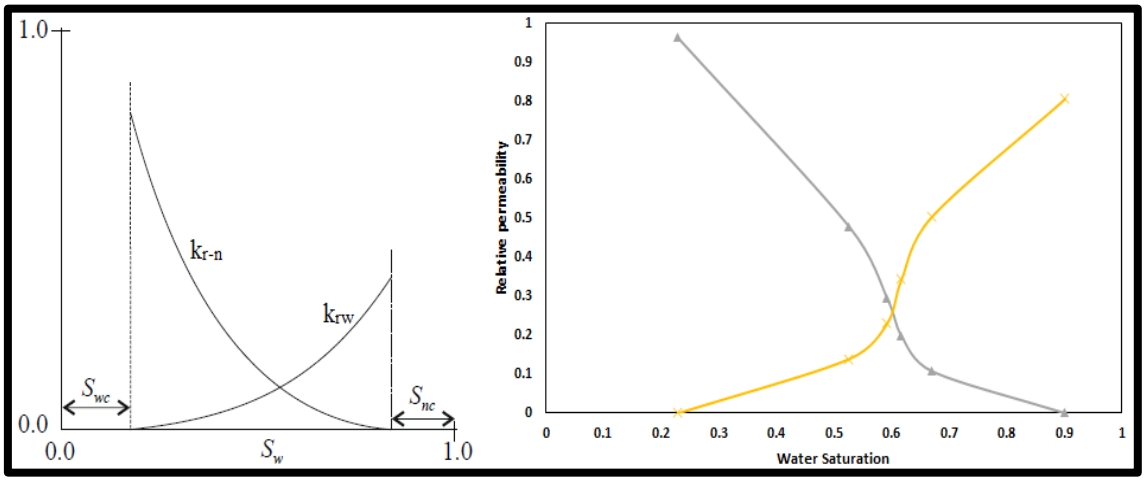


Figure 7: Typical Relative Permeability curves for two-phase flow (Left). Relative permeability curve for a resin coated sand proppant pack (Right). S_w, wetting phase. S_n non-wetting phase. S_{wc}, connate saturation, wetting phase. S_{nc}, connate saturation, non-wetting phase. k_{rw}, relative permeability of wetting phase. k_{r-n}, relative permeability of non-wetting phase.

Porosity

Porosity in a substance is a measure of empty or free space in that material. That free space may or may not be filled with other materials. Porosity is the part of net porous rock volume, which is not occupied by grains of rock, mud, cement, or any other material which constitutes the rock itself. In petroleum engineering, those spaces are often referred to as pores. There are two measures of porosity, absolute porosity, and effective porosity. Absolute porosity refers to the total pore volume for a rock, whereas effective porosity looks only at interconnected pores. A good reservoir rock would have lots of interconnected pores.

Porosity measurements are based on Boyle-Mariotte Law. The law states that the absolute pressure exerted by a given mass of an ideal gas is inversely proportional to the volume occupied by it at a constant temperature in a closed system.

Mathematically,

$$P \propto \frac{1}{V}$$

$$PV = c$$

Where, P is pressure exerted by the gas. V is volume occupied by the gas, and c is a constant.

Thus, to measure porosity of a sample, we can use it in the form of –

$$P_1V_1 = P_2V_2$$

P and V denote pressure exerted and volume occupied by gas at stage 1 and 2 respectively.

Permeability

Permeability is a proportionality constant, a measure that quantifies the ability of porous media to transmit fluids. It is a measure of flow capacity of a rock. Its unit of measurement, Darcy is named after Henry Darcy, the French engineer who first described it for flow of water through sand filters. Permeability in reservoir rocks is correlated with the rock's capacity to let fluid pass through a system of networked pores. If the pores are completely sealed, i.e. not connected to each other, they would represent an impermeable rock. Thus, presence of pores is not a sufficient condition for permeability. Its measurement often involves the use of Darcy's law, which incorporates flow rate, viscosity of flowing fluid, length through which flow occurs and the pressure gradient applied across the porous media to give a constant value.

$$k = v\frac{\mu . dx}{dP}$$

k, permeability of the porous media (S.I unit m^2).

v, superficial fluid flow velocity (m/s)

μ, dynamic viscosity of the fluid (Pa.s)

dx, length through which fluid flow occurs (m)

dP, pressure differential across the porous media (Pa)

For linear and horizontal flow of incompressible fluids at constant elevation, the Darcy's law in petroleum engineering is often represented as –

$$q = -A\,\frac{k}{\mu}\,\frac{dp}{dx}$$

Where, q represents the flowing rate of the fluid, A the cross-sectional area through which the fluid flows, and the minus sign "–" compensates for the negative pressure gradient in direction of flow.

This basic definition of permeability, can be adapted for utilization in innumerable conditions. One such adaptation, measuring permeability of samples by flowing compressed gases through them. In comparison with liquids, gases behave differently at pore scale. Darcy's law adapted for gases is –

$$q_0 = A\frac{k}{2\mu P_0}\frac{P_1^2 - P_2^2}{dl}$$

q_0, flow rate of gas at reference condition (usually atmospheric pressure and temperature).

P_0, reference pressure.

P_1^2, squared value of pressure at inlet (the point where gas enters the porous media).

P_2^2 is the squared value of pressure at outlet (the point where gas exits the porous media).

The best way to utilize Darcy's law, and measure permeability over a range of flow rates is to make a plot. A plot of $\frac{q}{A}$ versus $\frac{P_1^2 - P_2^2}{2.dl}$. With μ, P_0 being constant for a given system, permeability K can be easily calculated.

Darcy's law is inapplicable when the flow through the material is not laminar. This would generally happen at higher flow rates, where the associated Reynolds number is greater

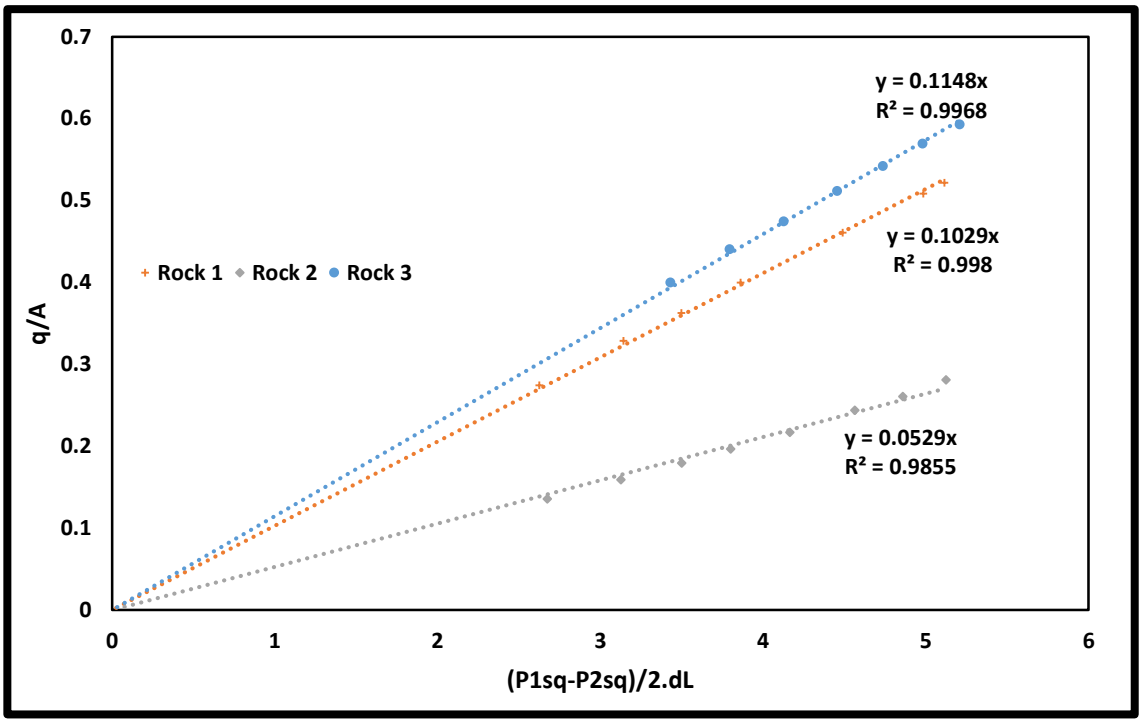


Figure 8: Gas Darcy Law plot for 3 rock samples. (Permeability of 0.94 mD, 1.83mD, 2.04 mD, measured using Nitrogen gas)

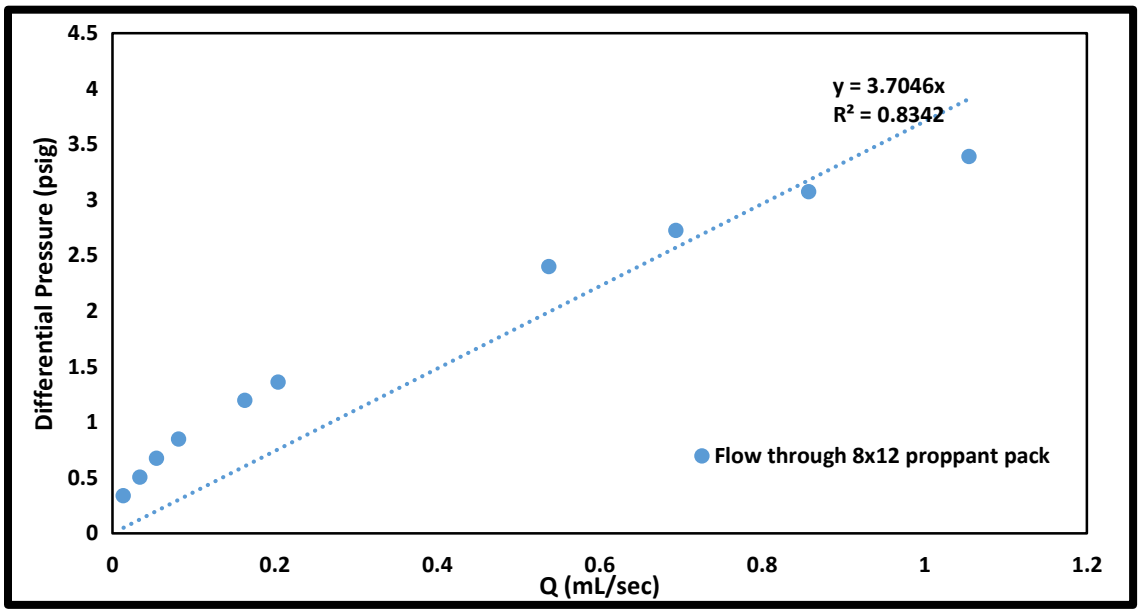


Figure 9: Darcy plot for non-Darcy flow through a proppant pack.

than 10. The increased fluid velocity inflicts a pressure drop which is greater than the

proportional velocity increase. This phenomenon is known as turbulent flow. It is associated with energy loses, which are not incorporated in the Darcy's law. Such flow behavior may also be referred to as non-Darcy flow. Measuring permeability for high permeability rocks can result in Reynolds number being greater than 10 for the porous media. In such a situation, non-Darcy flow is expected, and the Darcy plot, as plotted in Figure 9, does not remain a straight line passing through origin, Figure 8.

This was an issue while measuring liquid permeability of proppant packs. Thus, a different model to reliably measure permeability was required. Non-Darcy flow regime investigations by several authors were considered. The Forchheimer Equation for Non-Darcy flow in porous media has been reliably established. Hence, it was used for the non-

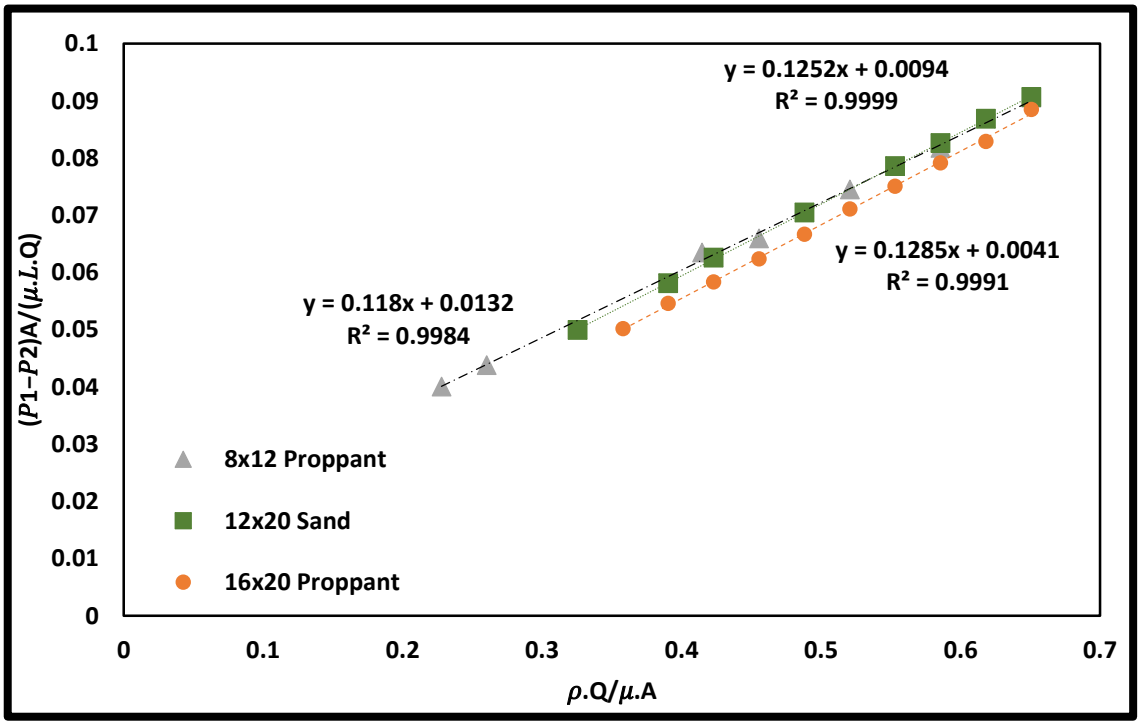


Figure 10: Forchheimer Plot for three different proppant packs

Darcy flow calculations in this work. (Evans, 1994) investigated non-Darcy flow through gravel packs in his dissertation. The author concluded that in presence of varying partial

immobile liquid saturation substantially increased the magnitude of non-Darcy flow coefficient in proppant packs.

Forchheimer proposed an equation capable of describing fluid flow at higher velocities, where the Darcy equation fails (Evans, 1994). For homogenous, one dimensional steady flow of an incompressible fluid in an isotropic porous media, the Forchheimer equation can be integrated to – (Evans, 1994)

$$\frac{P_1 - P_2}{\mu . L . v} = \frac{\beta . \rho . v}{\mu} + \frac{1}{k}$$

Where, β is the Forchheimer coefficient, and other letters are as defined earlier.

A plot of $\frac{P_1 - P_2}{\mu . L . v}$ versus $\frac{\rho . v}{\mu}$ will linear, with a slope, β and intercept $\frac{1}{k}$. Proppant pack flow data was analyzed with this equation. It was found, that Forchheimer equation was best suited for our analysis, and it gave repeatable results with minimum error. Figure 10 is an example plot of experimental data, which is in good agreement with the Forchheimer equation. The Forchheimer equation is not perfect, it is inapplicable at very high flow rates and it overestimates permeability (Barree & Conway, 2004). The work done in this thesis does not deal with very high flow rates, the data was linear on a Forchheimer plot. Additionally, this work is concerned with comparing permeability values, rather than absolute permeability tests. Thus, it was determined, to ease analysis, Forchheimer equation was selected for its simplicity.

On the other end of spectrum, are very low flow rates encountered while measuring gas permeability through tight rocks. In such situations, Klinkenberg effect comes into play. In 1941 Klinkenberg published a study, where he demonstrated that under steady state

and laminar flow conditions permeability of the porous media to gases can be approximated by a linear function of reciprocal of pressure. The effect he postulated was due to molecular interactions at the pore scale. With the Klinkenberg correction incorporated, it is possible to accurately measure permeability of very low permeability cores using gas pressure. Klinkenberg effect is active when the mean free path of the gas and the size (diameter) of the pore channels is comparable, there exists a maximum permeability limit for Klinkenberg effect (Zolotukhin & Ursin, 1997). Additionally, Klinkenberg effect is critical under 50psi mean pressure, and since the experiments were conducted at mean pressures greater than 60psi, Klinkenberg correction was not implemented.

Treatment Mechanism

Wettability modifiers investigated in this work are fluorinated nano-silica particles, which can permanently bond with quartz and carbonate substrates. Fluorine atoms being the most electronegative elements, can bind tightly to carbon atoms in organic molecules. Modest fluorination of molecular structure lead to extensive alteration of both physical and chemical properties. Fluoro-organics can exhibit extreme hydrophobicity, high thermal and oxidative stability, weak intermolecular interactions, low surface energy and remarkable biological inertness (Pagliaro & Ciriminna, 2005). Fluoroalkylsilanes are a group of synthetically manufactured organic compounds containing alkyl groups which have had all their hydrogen atoms replaced by fluorine. Silanes are inorganic compounds, with the first base unit, Silane SiH_4. Fluoroalkylsilane can exhibit formation of long chain polymeric networks. Presence of fluorine atoms on outer edges of molecular structures and multilayered formation is what imparts these compounds with their excellent hydrophobicity. Hydroxyl groups attached to silicon atoms (Silanes), exhibit strong chemical bond formation with rock substrates, thus exhibiting excellent chemical and thermal stability. The primary active compounds utilized in this work were Tetraethylorthosilicate [$Si(OC_2H_5)_4$] (Figure 11, abbreviated TEOS) and Triethoxy-1H,1H,2H,2Hperfluorodecylsilane [$CF_3(CF_2)_7(CH_2)_2Si(OCH_2CH_3)_3$] (Figure 11, abbreviated PFDS), both purchased from Sigma-Aldrich. The reaction mechanics, followed the sol-gel process. Sol-gel process involves conversion of monomers into a colloidal solution, which can then form polymeric networks (Sharifzadeh et al., 2013). The first step of the reaction involved hydrolysis of alkoxy group of TEOS in acidic conditions. Second, hydrolysis reaction of PFDS in acidic conditions. Acidic conditions

aided in rapid hydrolysis. Previous hydrolysis reactions lead to the formation of multiple silanol structures, Figure 12. These structures polycondensed to form the polymeric network (polymeric networks formed after monomers, dimers and trimers) depicted in

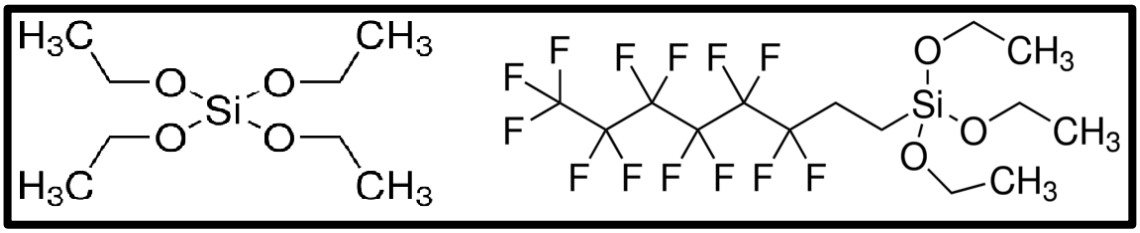


Figure 11: Molecular structure of TEOS (left) and PFDS (right) (Sigma-Aldrich, Product no. 667420 and Product no. 131903)

Figure 13. At this stage, the treatment was applied. $SiOH^+$ and $CaOH^+$ species present on rock substrates reacted with silanol groups of the formed polymers. This lead to the

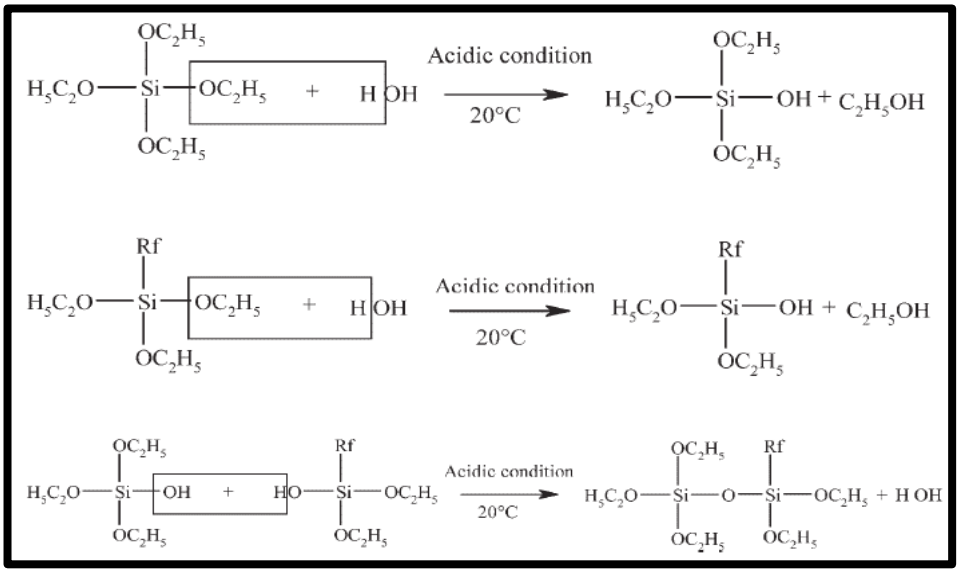


Figure 12: Chemical reaction between PFDS and TEOS (Sharifzadeh et al., 2013)

formation of strong molecular bonds between rock substrate and the polymer (Sharifzadeh et al., 2013). Post flush/cleanup of carrier phase (ethanol), the polymer remained bonded on the rock substrate. TEOS in this process increased density of reaction sites within the polymer, which helped form additional bonds between the polymer and

rock substrate, thereby the durability of the treatment was increased (Sharifzadeh et al., 2013).

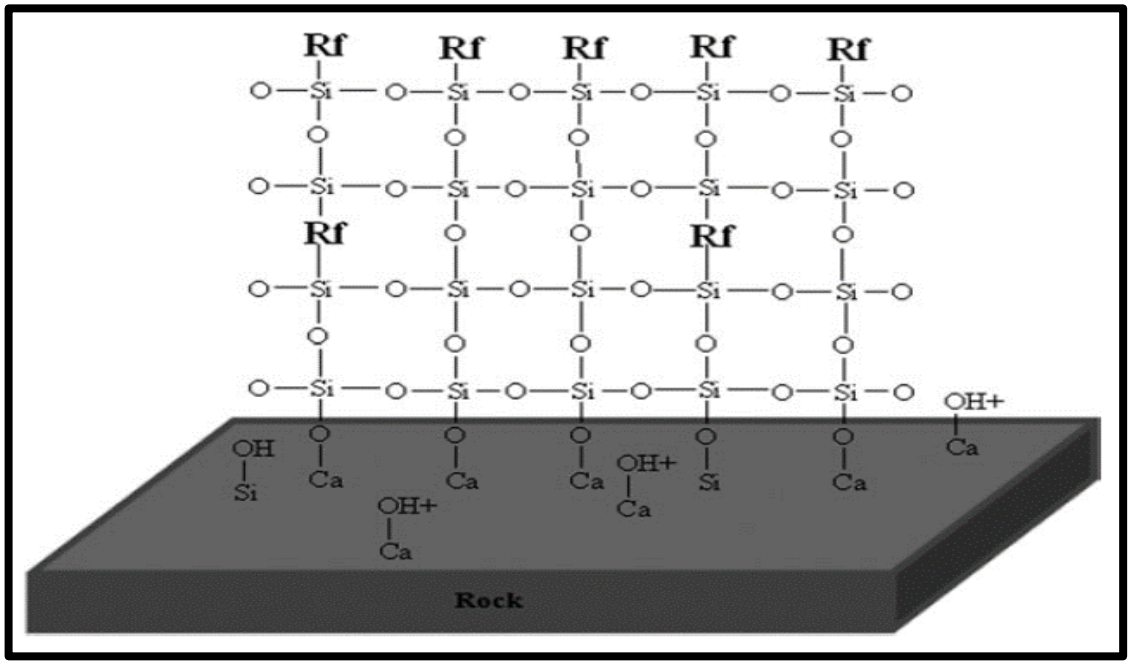


Figure 13: Schematic of rock substrate treated with PFDS and TEOS (Sharifzadeh, Hassanajili, & Rahimpour, 2013)

Proppant pack flooding

Proppant flooding experiments were conducted with an aim of studying the effect wettability alteration of proppants. To this end, experiments were conducted to obtain relative permeabilities of proppant packs and the experimental data of relative permeability was used simulated in CMG to observe the effect on production.

The experiments were started with various proppants, ranging in size from 8x12 US mesh size to 50x80 US mesh size. The larger proppants, 8x12, 12x20, 16x20 demonstrated non-Darcy flow behavior, Figure 9. Thus, Forchheimer equation was used to calculate permeabilities for sand packs.

Method for developing relative permeability tables involved conducting two-phase flow experiments at different flow combinations. For example, experiments were run with various combination of oil (Decane, NC10) and water rates, with net flow rate of 50cc/min. This rate was selected based on expected flow velocities in a 0.2-inch wide fracture, based on 1000 US barrel of oil per day production. In between each step, the setup was weighed to obtain change in weight at equilibrium conditions. More details about this are presented in experimental design and methodology.

Experiment Design and Methodology

Experiments were conducted with aim of first quantifying rock properties, second replicating the treatment proposed by (Sharifzadeh et al., 2013), and finally treating the rocks and studying the effects of proposed treatment.

The rocks, 12-inch long and 1-inch in diameter, Grey Berea and Indiana limestone outcrop samples were purchased from Kocyrek Industries. The long samples were cut into smaller 2-inch samples and edges were polished to achieve a flat-smooth surface.

The equipment for testing was either designed and developed in-house (Porosity meter) or purchased (Accumulator, Isco pumps and hassler-type core holder). Fittings and pressure transducers (valves, connectors, tubing) were purchased from Swagelok. Mettler-Toledo balance (MS-104S with accuracy of ±0.0001g) was used to weigh the core samples.

Chemicals for treatment design and testing were purchased from Sigma-Aldrich.

Contact angle measurement

The contact angle measurement setup consisted of a volumetric syringe, an elevated platform and a digital camera connected to a computer. The volumetric syringe enabled precise droplet volume control. The camera had an additional +10D macro lens attachment, which allowed us to obtain close-up photographs of droplets for drop shape analysis. Figure 14 is a picture of the contact angle setup.

Contact angle measurement steps –

1. Droplet of 10µL was placed on rock/glass surface.
2. Camera was programmed to capture images at 0, 3 and 10 seconds.

3. The images were then analyzed through a software, ImageJ. The software allowed relative measurement of length and width of the droplets.
4. Length and width data was converted to contact angles, by the using the arctan method described in the theoretical background.

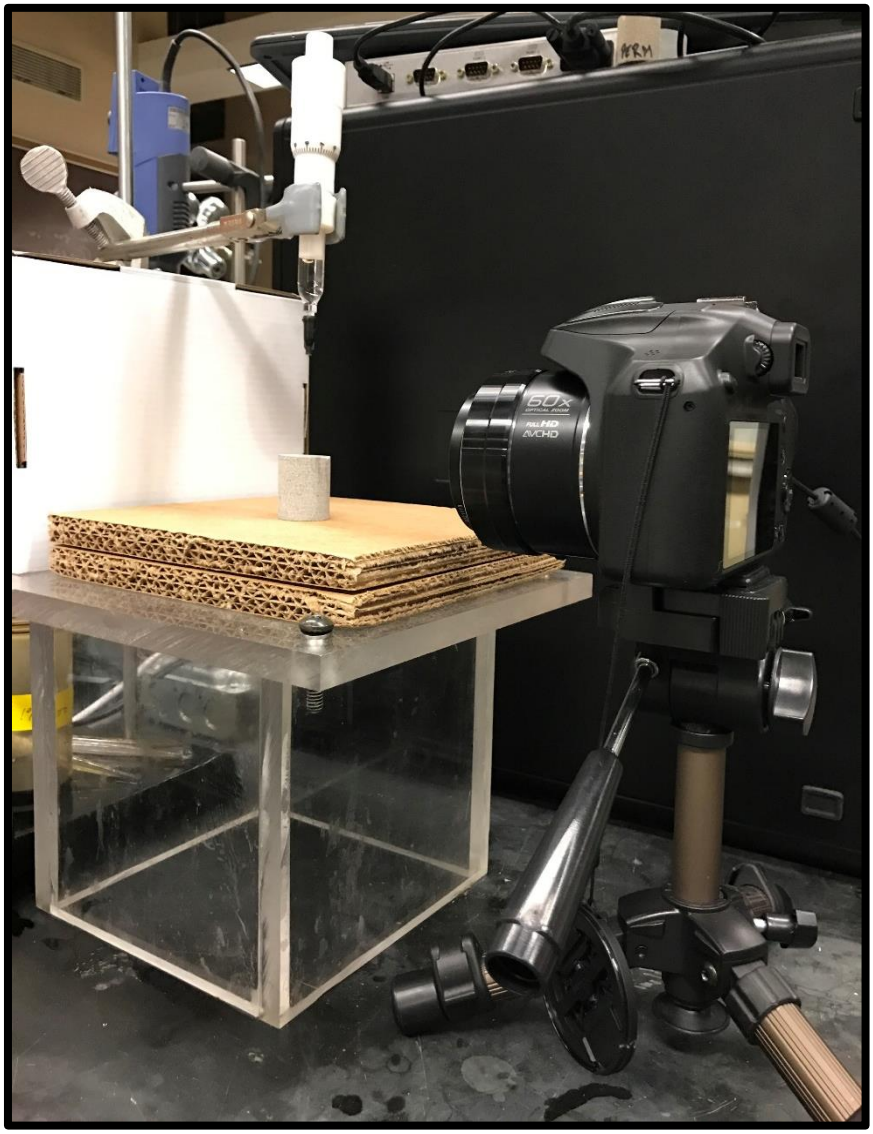


Figure 14: Contact angle measurement setup.

The level of surface during image capture was kept such that the edge appeared like a straight line. This allowed for consistency in captured images, and repeatable results. Images captured without insuring this, were inconsistent, since droplet height and width

when viewed in a 2-dimensional plane varied with slight variations in image capture angles.

Sample calculation in Microsoft Excel –

Table 1: Contact angle sample calculation.

W	H	Water/Decane	Contact angle (Radians)	Contact Angle (Degree)
165	137	Water	2.057536498	117.89
Formula			=2*ATAN(H*2/W)	

Preparation of core samples

Fresh cores were first cut to 2-inch sample length. The cut cores were then polished to achieve a flat surface, followed by 6hrs in a drying oven at 100^{o}C. Length and diameter were measure at 10 different points to have accurate dimensions. Weight of the core samples was monitored through various stages of tests and treatments.

One 12-inch long, 1-inch diameter rock core of Grey Berea (Sandstone) was cut to give GB1, GB2, GB3* (Asphaltene deposited), GB4, GB5 and GB6. One 12-inch long, 1-inch diameter core of Indiana Limestone was cut to give LS1, LS2, LS3, LS4, LS5, and LS6.

Table 2: Rock samples (untreated and treated) information

Untreated	Treatment A (PFDS-1)	Treatment B (PFDS-2)
GB4, GB3*, LS4, LS2	GB1, GB5, LS1	GB2, LS3

Porosity meter

The porosity meter was designed in-house to be able to hold samples ranging from 0.1-inch length to 6-inch length, with a diameter of 1-inch. The core holder contained 7 solid stainless steel spacers measuring 2.5 inch, 1.5 inch, 1 inch, 0.5 inch, 0.25 inch, 0.15 inch

and 0.1 inch in length, and 1-inch in diameter. These were labeled 1 through 7. The pressure transducer was a Swagelok 0-50 psi range transducer.

As outlined in the theoretical background, porosity measurements were based on Boyle's law. The entire system, except the core holder and half of the first valve (Figure 15 schematic, in red-box) were denoted by volume V_1 and the volume inside the red box was denoted by volume V_2. To achieve accurate results, the porosity meter was first calibrated with the solid spacers. P_1V_1 and P_2V_2 were measured for each combination of spacers inside the core holder and an excel sheet was prepared, to enable easy porosity measurement with calibrated data. The excel sheet required length, diameter, weight, P_1,

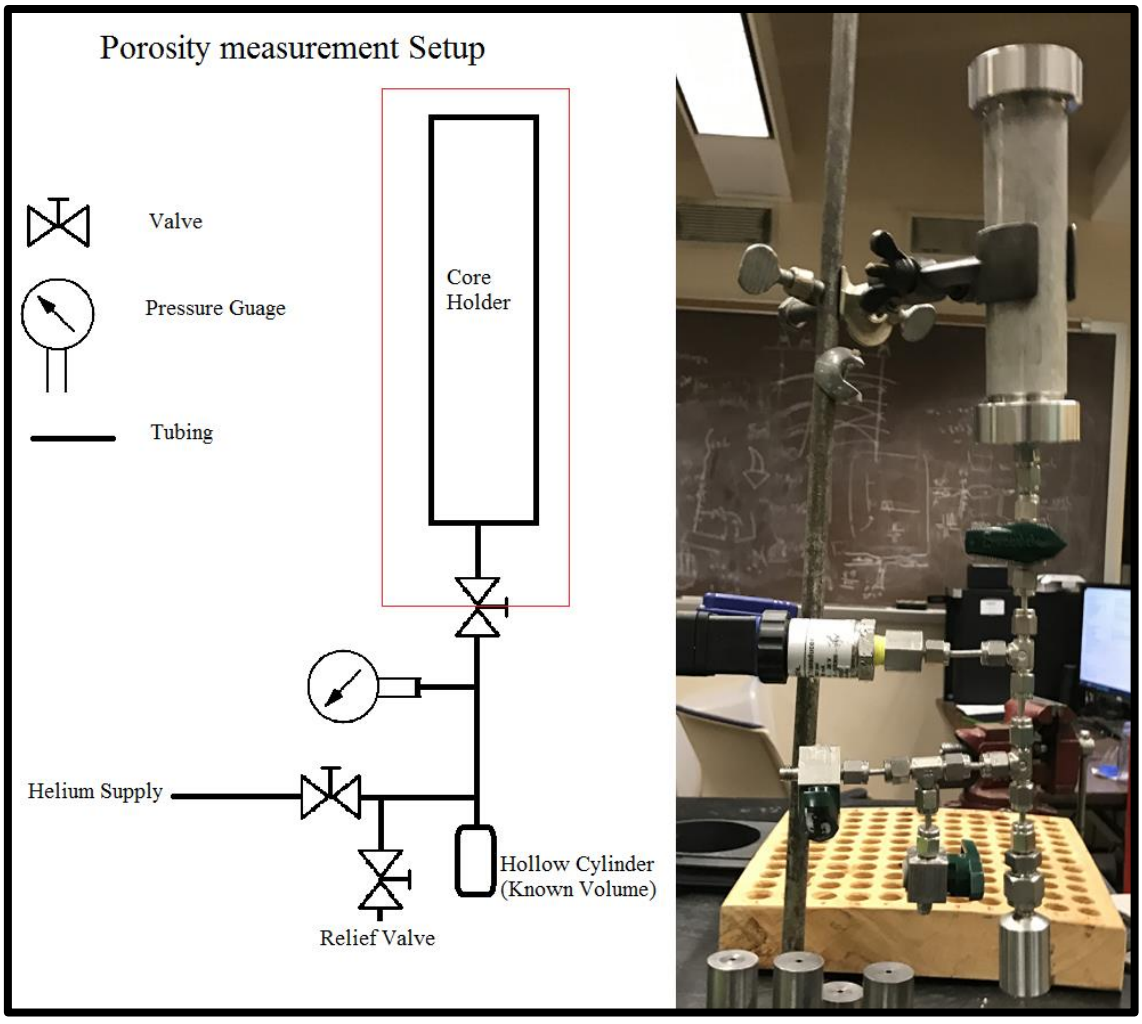
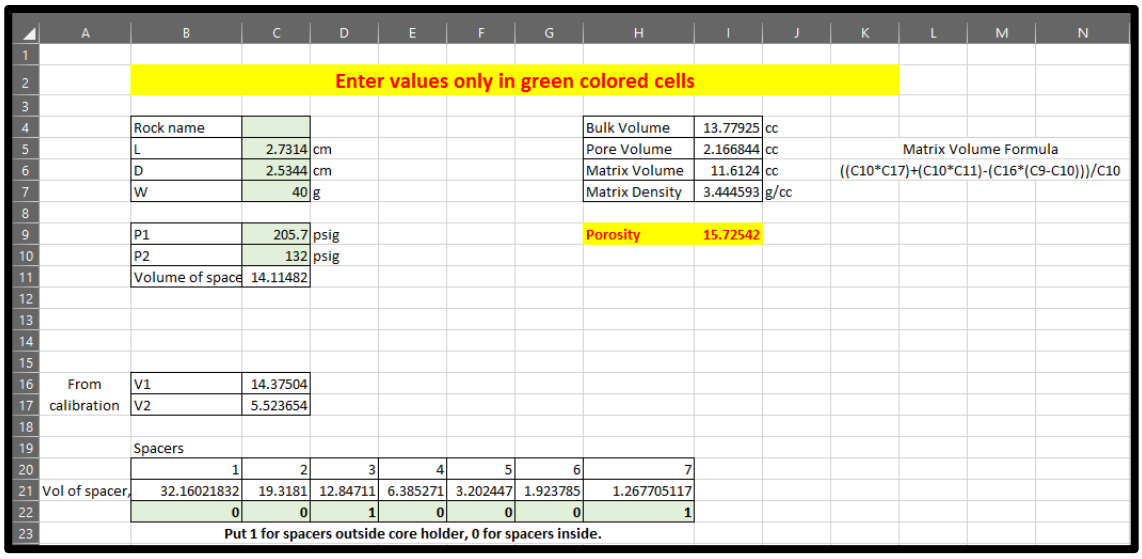


Figure 15: Porosity meter (Schematic, left. Picture right)

P_2 and designation of the spacers kept out to calculate porosity, bulk density, pore volume and matrix density.

Steps for measuring porosity –

1. Length, diameter, and weight of sample were measured.
2. Spacers were removed from core-holder.
3. Spacers and sample were stacked side by side.
4. A combination of spacers, such that they were just barely taller than the sample itself, when stacked side-by side on a flat surface was selected. This was done to minimize the empty space inside the core-holder.
5. Keeping the selected combination of spacers out, remaining spacers and core sample were loaded into the core holder.
6. Before charging with helium, it was made sure all that valves were shut, and the caps of core holder were screwed tight.
7. System was charged with Helium gas, to 200 psi (or any other required pressure).
8. Helium supply valve was shut-off, followed 1-minute waiting period for pressure stabilization.
9. Initial pressure, P_1, was recorded.
10. Valve connecting the core holder to rest of the system was opened, followed by 1-minute waiting period for pressure stabilization.
11. Final pressure P_2, was recorded.
12. Pressure was released from the system via relief valve.
13. Core sample was unloaded, and spacers replaced.



	A	B	C	D	E	F	G	H	I	J	K	L	M	N
1														
2		Enter values only in green colored cells												
3														
4		Rock name						Bulk Volume	13.77925	cc				
5		L	2.7314	cm				Pore Volume	2.166844	cc	Matrix Volume Formula			
6		D	2.5344	cm				Matrix Volume	11.6124	cc	((C10*C17)+(C10*C11)-(C16*(C9-C10)))/C10			
7		W	40	g				Matrix Density	3.444593	g/cc				
8														
9		P1	205.7	psig				Porosity	15.72542					
10		P2	132	psig										
11		Volume of space	14.11482											
12														
13														
14														
15														
16	From	V1	14.37504											
17	calibration	V2	5.523654											
18														
19		Spacers												
20		1	2	3	4	5	6	7						
21	Vol of spacer,	32.16021832	19.3181	12.84711	6.385271	3.202447	1.923785	1.267705117						
22		0	0	1	0	0	0	1						
23		Put 1 for spacers outside core holder, 0 for spacers inside.												

Figure 16: Sample porosity calculation from MS Excel

Imbibition setup

The imbibition setup consisted of the Mettler-Toledo MS104S, which has an accuracy of ±0.0001g. The balance was places on stand, with a hole in the bottom. A fishing line was hooked from the bottom weighing attachment of the balance. The core samples were then attached to the fishing line for continuous weight recording. The balance, connected to a computer recorded data every 3-seconds.

Steps for generating imbibition curves –

1. A dried core at room temperature was selected.
2. The length, diameter and weight of sample were measured.
3. Porosity of sample was measured to obtain pore volume.
4. Fluid densities were recorded from literature (Air at room temperature, Decane/Water at room temperature)
5. The fishing string was tied around the sample securely.

6. Weight of the sample, in air, with the string attached was recorded.
7. Next the sample string and, the fishing string with the balance were connected, via a hook.
8. It was made sure at this point, that the computer started recording weight data at 3-second intervals.
9. With a stopwatch in one hand, the sample was dropped into a beaker filled with either decane or water, and the stopwatch was started simultaneously. This made sure that a clear starting time for imbibition was available, since the computer at this point had already been recording data.

	A	B	C	D	E	F	G
1							
2	Date	5/19/2016					
3	Rock	GB-J1-2					
4	History	Grey Berea sample (GB-J1-2). The 12 inch sample was cut in 6 peices by					
5		Followed by 24hrs drying in oven at 100 degC. 2 runs of contact angle m					
6							
7	L	4.8612	cm				
8	D	2.5314	cm	52g, untreated weight			
9	W	52.012	g	treated weight			
10	Porosity	0.20379	fraction				
11	Pore Volume	4.985834	cc				
12	Permeability	109	md				
13							
14	Fluid 1 (displaced)	Air	0	g/cc			
15	Fluid 2 (displacing)	Water	1	g/cc			
16							
17	W, with wire in air, initial	52.063					
18	W, with wire in air, final	53.171					
19	W, with wire in fluid, final	28.862	Last reading in fluid				
20	F, Buoyancy	24.309	B18-B19				
21	W, with wire in fluid, initial	27.754	B17-B20				
22	W final, no wire	53.082					
23	Final saturation	0.214608	((B22-B9)/(C15-C14))/B11				
24	Stop watch time	12					
25	Computer time	171					
26	Time zero	159					
27							
28		GB-J1-2 treated, water imbibition, 1					
29		Time (sec)	Weight (g)	Time (min)	Recovery (fraction)		
30		0	52.233	-2.65	=(C30-$B$21)/($C$15-$C$14)/$B$11		
31		3	52.25	-2.6	4.91312		
32		6	52.478	-2.55	4.95885		
33		9	-1.425	-2.5	-5.85238		

Figure 17: Sample Calculation for imbibition recovery fraction.

10. Spontaneous imbibition was allowed to happen undisturbed, until no weight change was observed over a 3hr period. Time to equilibrium varied from ~14hrs

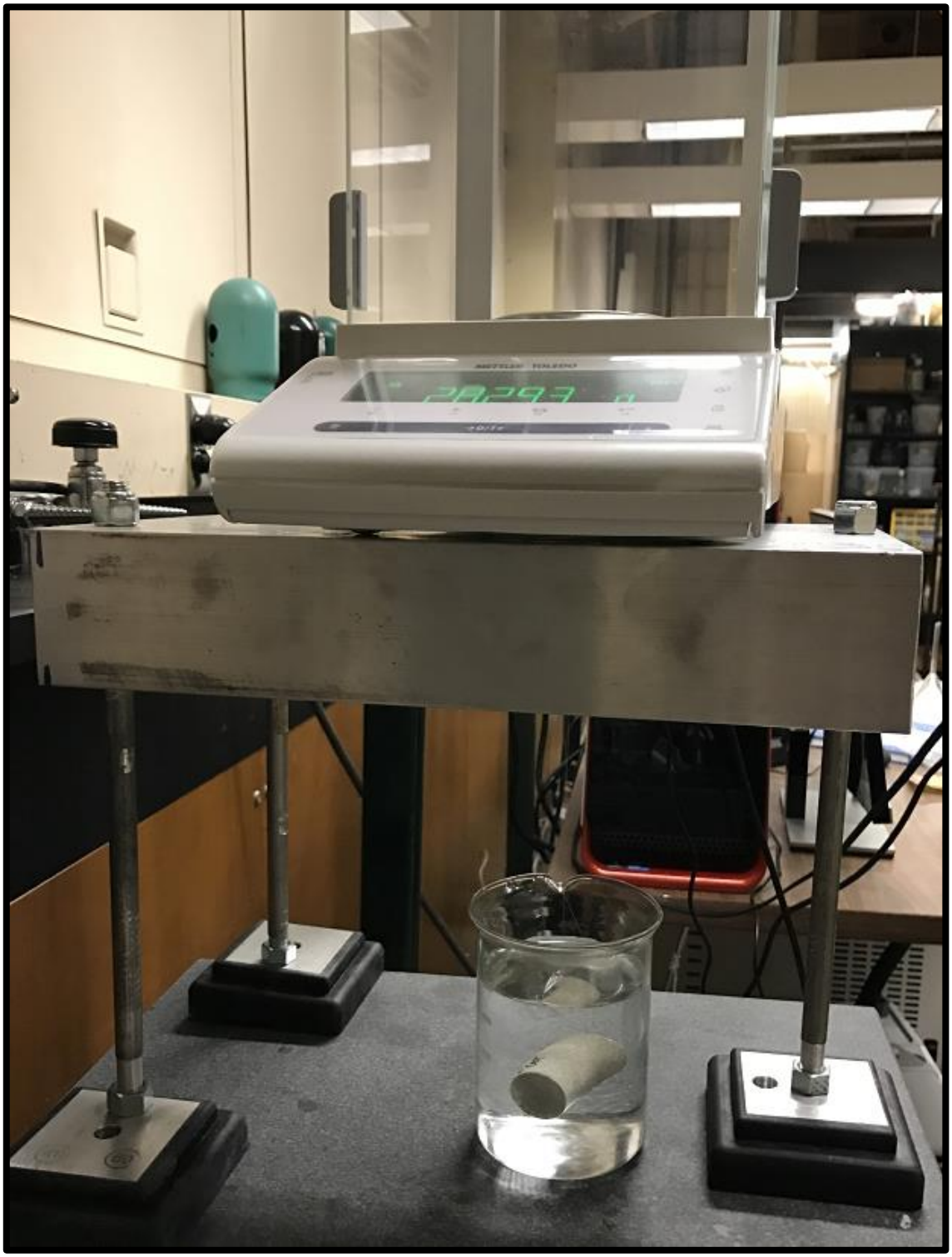


Figure 18: Imbibition setup

for sandstone samples to ~60hrs for limestone samples.

11. The weight reading, with the sample suspended in fluid, at end of imbibition was recorded as final weight of sample with wire in fluid.
12. Next the sample was taken out from the fluid, its surface was dabbed with non-absorbing paper to remove excess fluid from surface. It was then weighed, and recorded as final weight with wire in air.
13. The wire/fishing string was removed and the sample was weighed again, recorded as final weight in air, without wire.

Permeability measurement

Permeability measurements were done by holding the core samples in a hassler type core holder, at a confining pressure of 1600 psi. the core holder was capable of handling cores of 1-inch diameter, length from 0.25-inch to 12-inch. For the shorter cores, a series of spacers with a bore through the center were available. A schematic of the permeability

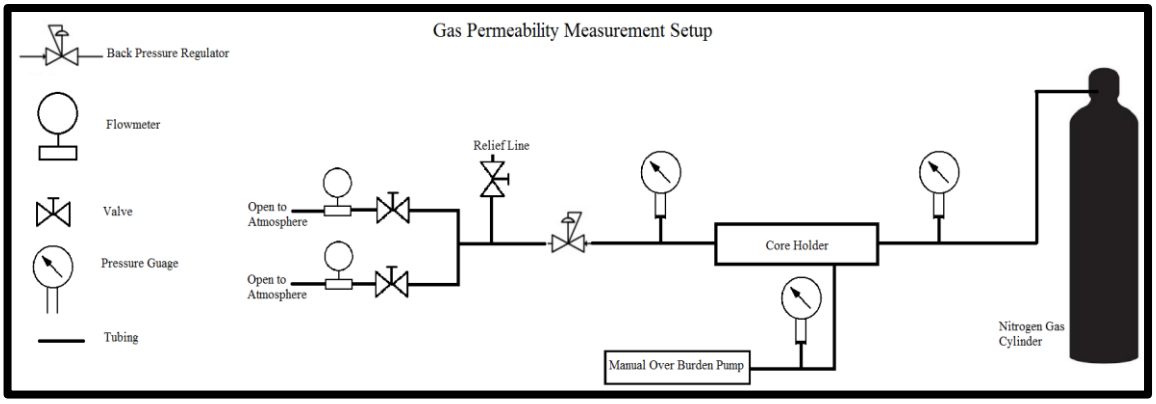


Figure 19: Setup to measure gas permeability.

setup is represented in Figure 19. Theoretical background section covered measurement of permeability.

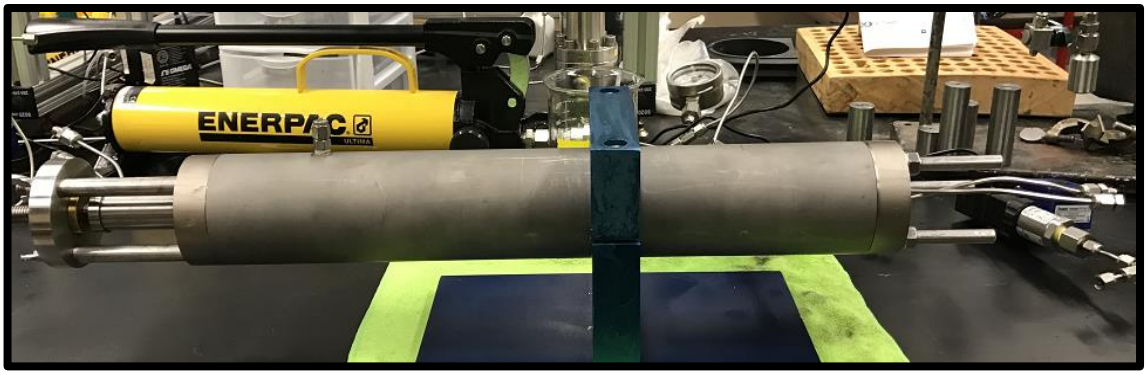


Figure 20: Picture of Hassler type core-holder on a stand

There were Swagelok pressure transducers (0-300psi range) at both inlet and outlet of the core holder, which enabled measurement of respective pressures. A pressure gauge (0-2000psi range) was also present between the overburden pump (ENERPAC hydraulic pump) and the core holder. A back-pressure regulator at the outlet from core holder enabled precise control over the outlet pressure. Two digital volumetric flowmeters

(OMEGA FMA-1600 series), were connected back-pressure regulator. The flowmeters operated in different ranges, 0-20 SLPM and 0-2 SLPM (standard liters per minutes). This allowed for measurement of both low and high permeability rocks, without damaging the flowmeters.

Steps for measuring permeability –

1. The first step was always to make sure that core holder did not have any pressure.
2. Porosity data from porosity measurement was used.
3. The outlet cap (left hand side) was unscrewed and the core was loaded in. The core was always made sure to be loaded before spacers. This was done, so as to have the core in contact with the inlet. The inlet was designed with multiple holes and channeled troughs to distribute inlet fluid evenly.
4. The spacers were loaded next and the outlet end-cap was screwed back on.
5. The adjustable piston was tightened, to make sure that the core and the spacers were securely held between the end-caps.
6. Confining pressure was applied and held at 1600psi.
7. The relief line was opened and the valves to flowmeters were shut. This was done to control the pressure at outlet, since excess pressure could damage the sensitive flowmeters.
8. Nitrogen gas was flowed from the tank, and inlet pressure set to 100psi.
9. With the back-pressure regulator, outlet pressure was set to initially 50psi.
10. Next valve for the 0-20 SLPM flowmeter was opened, and then the relief valve was shut. If the flow was below 2 SLPM, the 0-2 SLPM range flowmeter was selected.

11. Pressures and flowrates were recorded after stabilization.

12. Back-pressure was increased to obtain new pressures and flow-rates.

13. Once the required number of readings were obtained, the gas supply was shut off.

14. Confining pressure was released, and the core was unloaded.

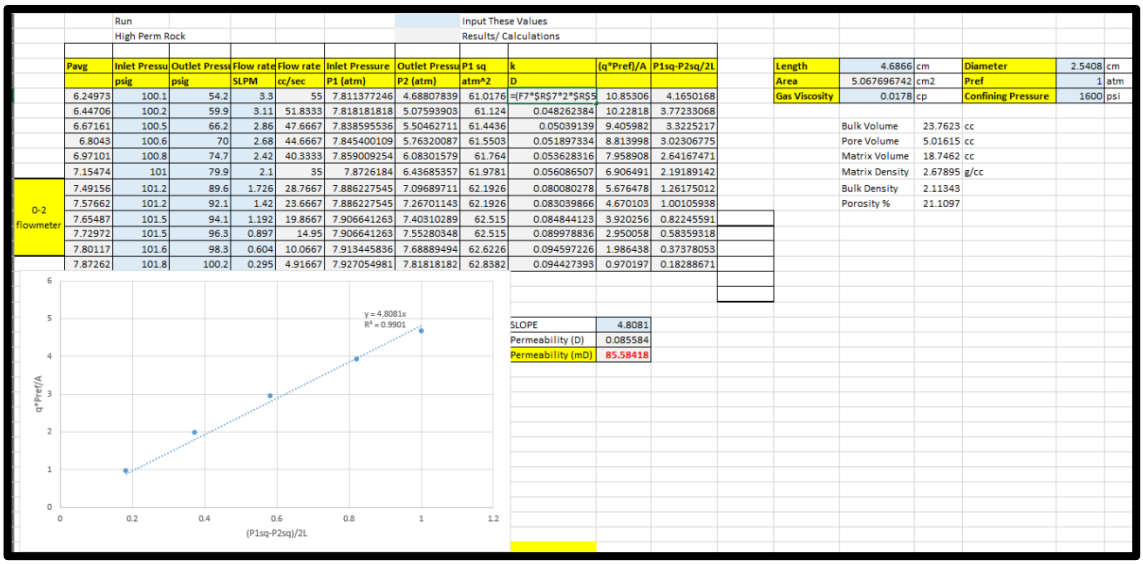


Figure 21: Sample Permeability Calculations

The permeability measurement setup for Darcy and non-Darcy was the same. Only the associated equations and plots changed, when switching to non-Darcy calculations.

Treatment design

Treatment mechanics are reactions were covered in theoretical background.

Table 3: Treatment chemicals

Chemical name		Sigma-Aldrich Product number	Chemical Formula
Triethoxysilane-1H,1H,2H,2H perflourodecylsilane	PFDS, 97% purity	658758-25G	$CF_3(CF_2)_7(CH_2)_2Si(OCH_2CH_3)_3$
Ethanol	99.8% wt	459844-4L	C_2H_6O
Tetraethoxysilane	TEOS, 98% purity	131903-1L	$Si(OC_2H_5)_4$
Hydro-chloric Acid	37 wt%	320331-2.5L	HCl
De-ionized Water	--	--	H_2O

Two separate treatments were done, by varying the ratio of reactants. Treatment A and Treatment B, tabulated in Table 4.

Table 4: Chemical ratios for Treatments A & B.

	Treatment A (PFDS-1)			Treatment B (PFDS-2)		
Reagent	Ideal weight (gm)	Weight (gm)	Weight Fraction	Ideal weight (gm)	Weight (gm)	Weight Fraction
TEOS	4	4.08	0.08	1	1	0.04
PFDS	1	1.07	0.02	0.25	0.26	0.01
EtOH	42.5	42.5	0.85	23	23.05	0.92
Water	2	2.06	0.04	0.5	0.51	0.02
HCl	0.5	0.54	0.01	0.25	0.27	0.01
Total	50	50.25	1	25	25.09	1

Synthesis of polymeric surfactant coating –

1. PFDS and TEOS were mixed in required ratio in a capped conical flask.
2. Ethanol was added at room temperature.
3. De-ionized water and HCl were subsequently added drop-wise to the solution over a period of 2 hours, while constantly stirring the solution. A magnetic stirrer at its lowest setting was used to stir the solution.
4. This led to the formation of a transparent sol-gel solution (Sharifzadeh et al., 2013).

Application of treatment to core sample was done using the hassler type core holder. The same core holder was used for permeability measurements. A core holder was used, instead of direct immersion, since that enabled application of confining pressure similar to reservoir conditions. An accumulator driven by an ISCO pump was used to pump the treatment through the core. The pressure gauges, back-pressure regulator and the

flowmeters were removed from the permeability setup. The effluent treatment fluid was collected for further study.

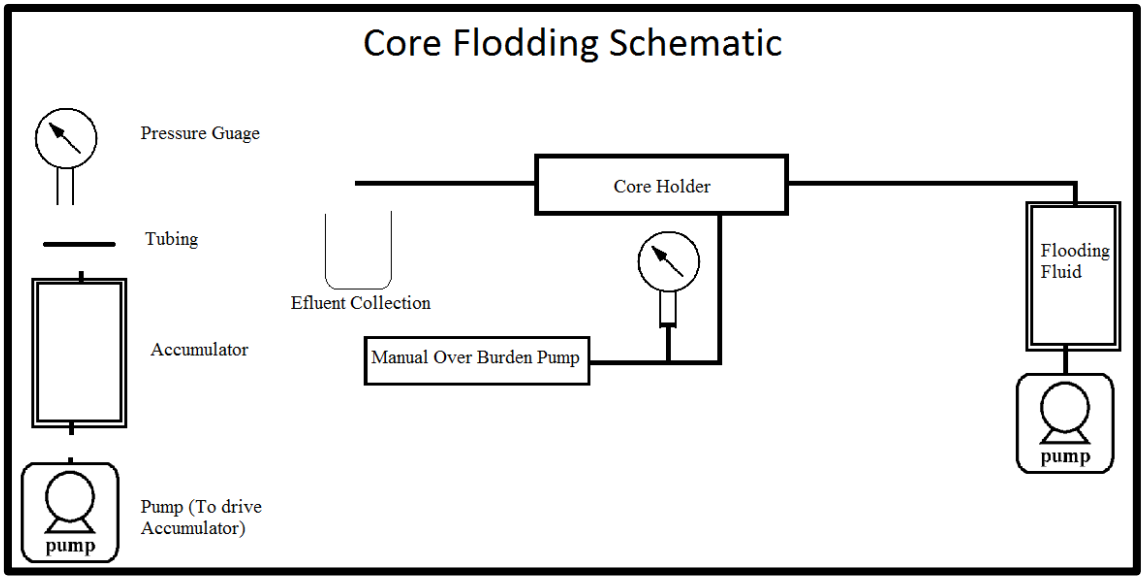


Figure 22: Core flooding/treatment setup

The steps involved with application were –

1. Treatment fluid was loaded into the accumulator, and air relieved from the system.
2. The core was loaded into the core-holder, spacers followed.
3. After securing both ends of the core-holder, confining pressure was raised to 1600psi. This step was done to insure a proper seal.
4. Approximately three pore volumes of treatment fluid (~20 mL) was pumped through the core at 1mL/min.
5. The effluent was collected, and the core left in the core holder for 24 hours.
6. After the aging period, nitrogen gas was pumped through the core, to cleanup remaining fluid.
7. The core was dried in the drying oven at 80^{o}C for 2 hours, to get rid if any remaining fluid.

8. After cooling, porosity, permeability, contact angle and imbibition tests were run on treated cores.

Proppant pack flooding

A hollow acrylic cylinder 1-inch in diameter and 9-inch length was used to pack the proppant. Wire mesh screens were used on both the inlet and the outlet, to prevent proppant movement after packing. A valve connected the sand pack to facilities vacuum line. Vacuum helped in eliminating air from the system, to achieve initial 100% fluid

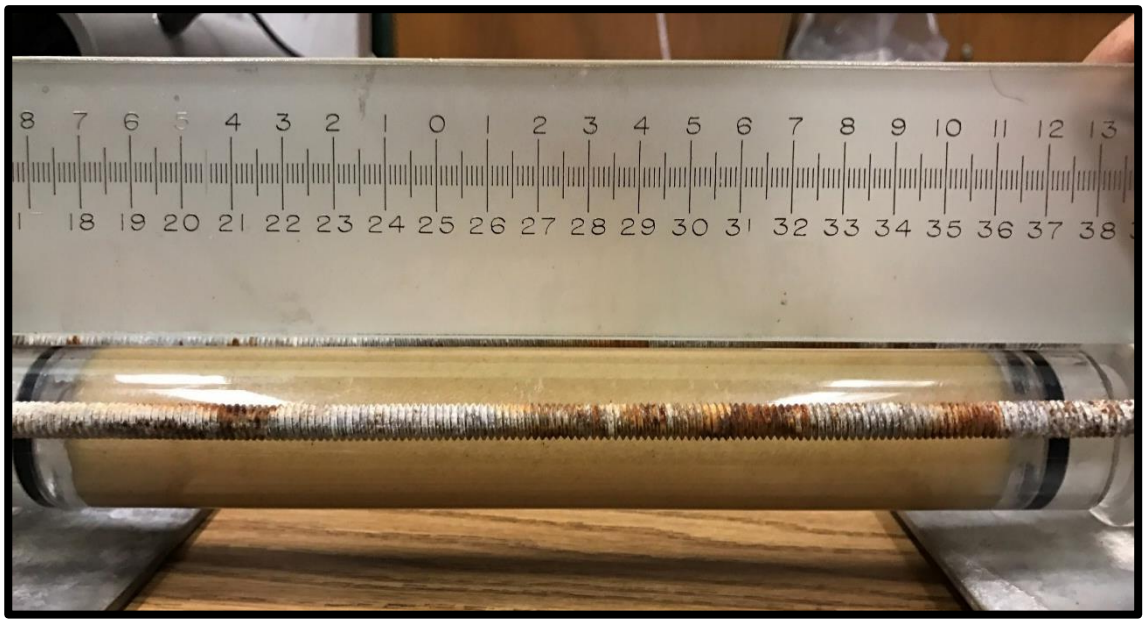


Figure 23: Proppant pack, 40x70 Sand

saturation. The effluent from the pack was collected and monitored, to aid in saturation calculations (generation of relative permeability tables). Two accumulators were at the inlet of the sand pack. One contained oil (Decane, NC10), the other de-ionized water. The accumulators were driven by Isco pumps. Simultaneous operation of the accumulators resulted in two-phase flow (oil-water), data from which was used to generate relative permeability tables. Figure 24 represents a schematic of the sand pack. Figure 25 and Figure 26 together show a picture of the sand pack setup.

Several different proppants were tested, the final tests were done using 40x70 sand and a 50x80 resin coated sand. This specific size distribution was selected to achieve reasonably

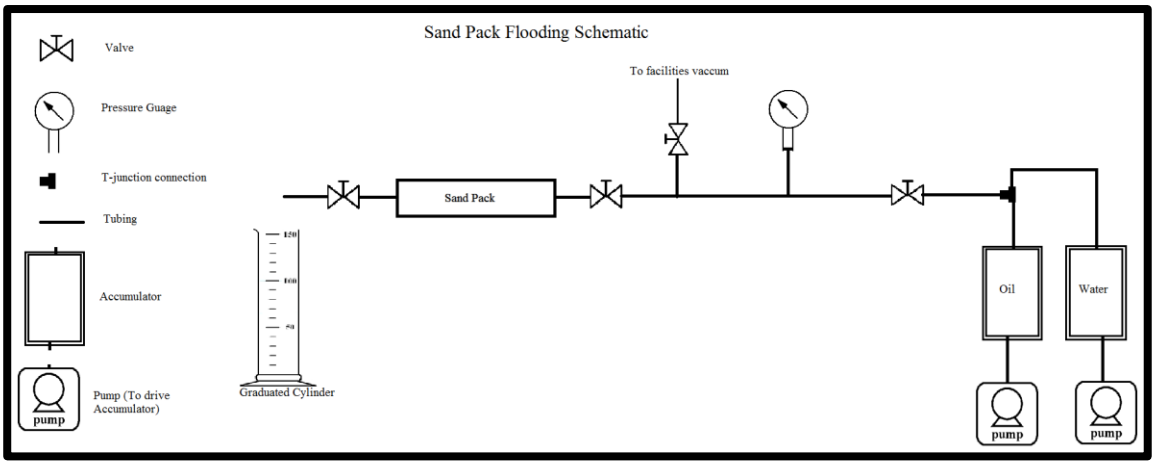


Figure 24: Sand pack setup schematic



Figure 25: Sand pack picture 1

high permeability values. Larger proppant sizes, for example a 12x20 ceramic proppant resulted in very small pressure build-up on the inlet, which led to inaccurate permeability calculations. The low pressure was not accurately detected by the Swagelok 0-300psi range transducer connected to the inlet, thus it was later switched out for a Swagelok 0-50psi range transducer. A clamping mechanism made sure that the end-caps were secure.

Steps for obtaining data to generate relative permeability tables –

1. Dry, empty weight of the hollow acrylic cylinder and the endcaps was measured.

2. Dead volumes of the end-cap were determined. Dead volume was the hollow volume in the endcaps which did not have any sand packed, because of the presence of wire mesh screens.
3. Sand/proppant was packed into cylinder. To achieve good packing, it continuously tapped, which imitated a shaker.
4. The packed cylinder was clamped, to secure the endcaps, and to make sure that the proppant was tightly packed.
5. The system was weighed again, thus the weight of packed sand was obtained.

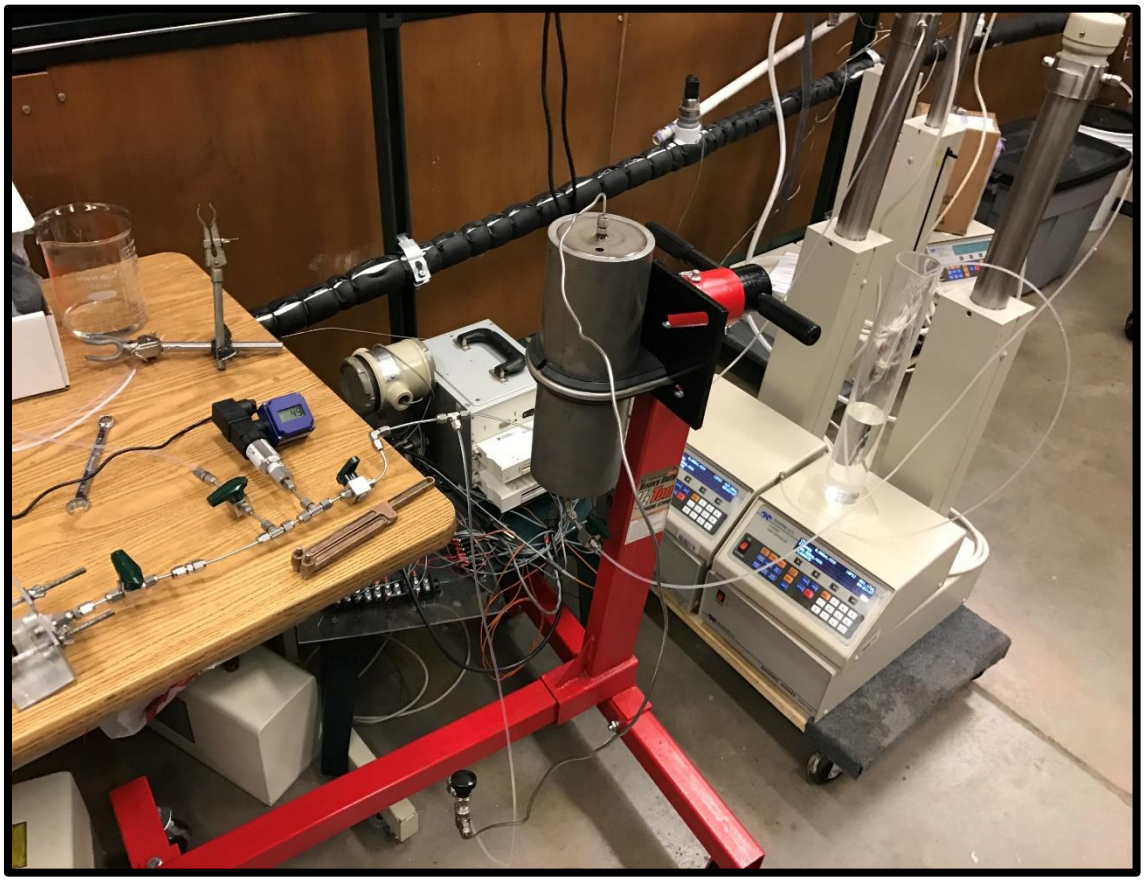
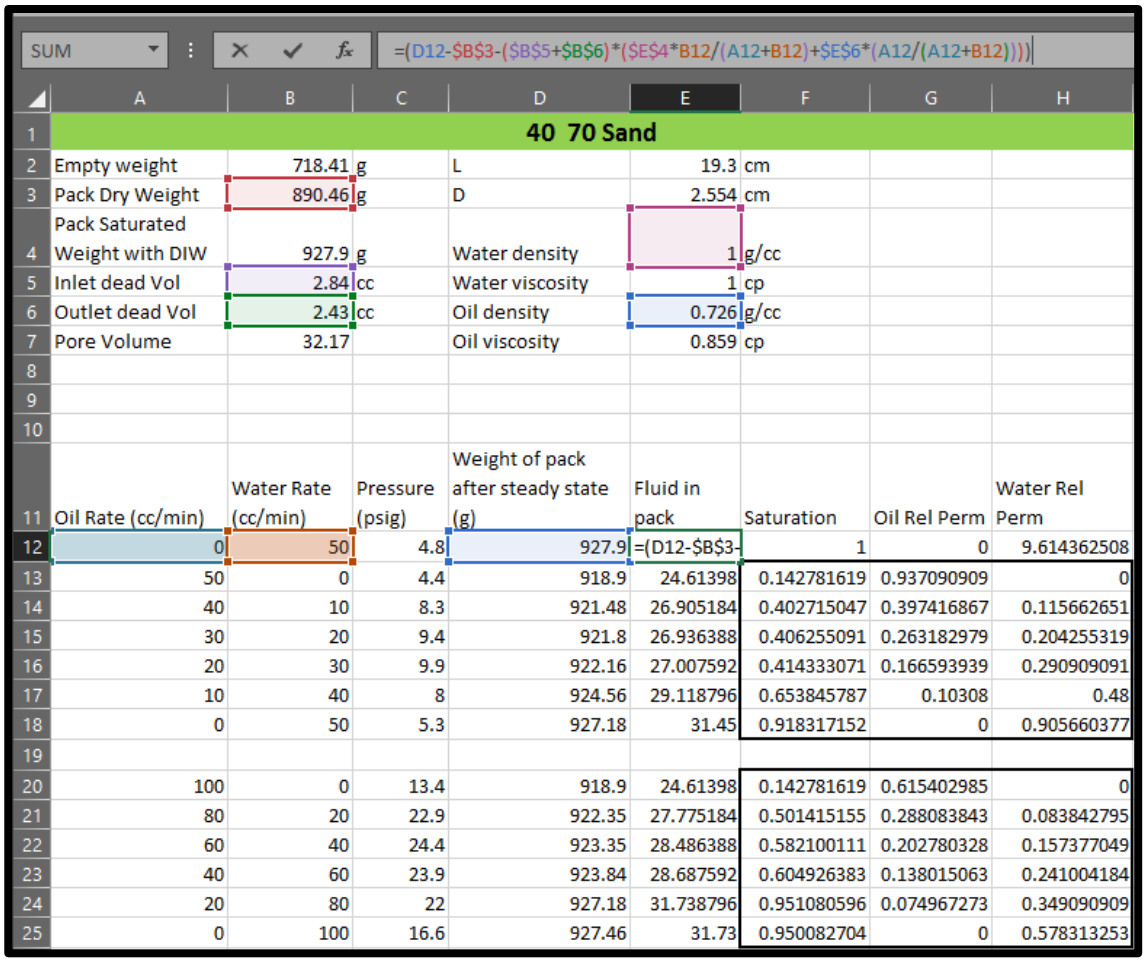


Figure 26: Sand pack picture 2.

6. Length of the packed sand column was measured, since it varied with each packing. Only the length packed with sand was considered. For example, between the 18 and 36cm mark in Figure 23.

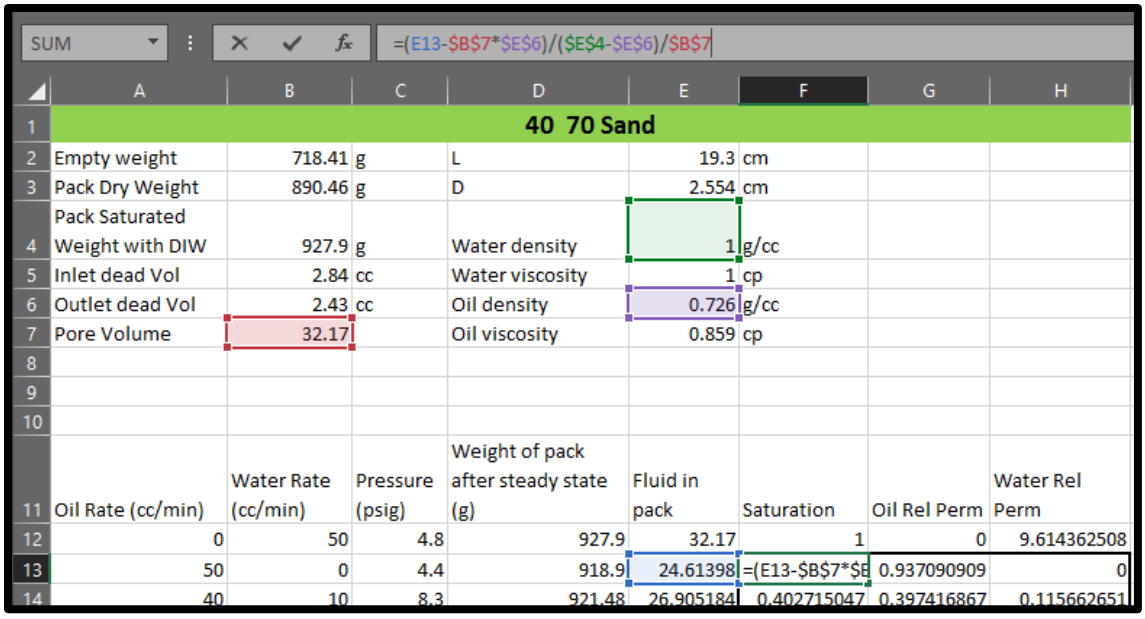
7. The system was then vacuumed and its weight measured.
8. Next, the system was saturated with water and weighed again.
9. With difference in weight, amount of water held in the system was calculated. With this and the endcap volume, porosity of the system was determined.
10. Water was passed through the system at various rates, to generate pressure and flow data. This data was used to calculate the permeability of the system (Non-Darcy permeability using Forchheimer equation. Application of Darcy equation to data from all sand pack flow studies indicated non-Darcy flow behavior).
11. Two-phase flow tests were conducted at two different rates. First, at 50cc/min of combined flow rate (oil and water), second at 100cc/min of combined flow rate. For example, after the permeability run with water, one test involved oil flooding at 50cc/min, until irreducible water saturation was achieved (Detected by pressure stabilization at inlet). Once steady state was achieved, the system weighed, to determine the change in weight. This was followed by a run with 40cc/min of oil and 10cc/min of water. Again, the system was weighed after steady state. Next, a run with 30cc/min of oil and 20cc/min of water. Similarly, a run at 100cc/min combinations for oil and water.
12. Relative permeability tables were developed from this data. A sample of calculations are shown in Figure 27, Figure 28 and Figure 29. Relative permeability of water was calculated as it was for oil, utilizing viscosity of water instead of viscosity of oil.



SUM | =(D12-$B$3-($B$5+$B$6)*($E$4*B12/(A12+B12)+$E$6*(A12/(A12+B12))))

	A	B	C	D	E	F	G	H
1	40 70 Sand							
2	Empty weight	718.41	g	L	19.3	cm		
3	Pack Dry Weight	890.46	g	D	2.554	cm		
4	Pack Saturated Weight with DIW	927.9	g	Water density	1	g/cc		
5	Inlet dead Vol	2.84	cc	Water viscosity	1	cp		
6	Outlet dead Vol	2.43	cc	Oil density	0.726	g/cc		
7	Pore Volume	32.17		Oil viscosity	0.859	cp		
8								
9								
10								
11	Oil Rate (cc/min)	Water Rate (cc/min)	Pressure (psig)	Weight of pack after steady state (g)	Fluid in pack	Saturation	Oil Rel Perm	Water Rel Perm
12	0	50	4.8	927.9	=(D12-$B$3-	1	0	9.614362508
13	50	0	4.4	918.9	24.61398	0.142781619	0.937090909	0
14	40	10	8.3	921.48	26.905184	0.402715047	0.397416867	0.115662651
15	30	20	9.4	921.8	26.936388	0.406255091	0.263182979	0.204255319
16	20	30	9.9	922.16	27.007592	0.414333071	0.166593939	0.290909091
17	10	40	8	924.56	29.118796	0.653845787	0.10308	0.48
18	0	50	5.3	927.18	31.45	0.918317152	0	0.905660377
19								
20	100	0	13.4	918.9	24.61398	0.142781619	0.615402985	0
21	80	20	22.9	922.35	27.775184	0.501415155	0.288083843	0.083842795
22	60	40	24.4	923.35	28.486388	0.582100111	0.202780328	0.157377049
23	40	60	23.9	923.84	28.687592	0.604926383	0.138015063	0.241004184
24	20	80	22	927.18	31.738796	0.951080596	0.074967273	0.349090909
25	0	100	16.6	927.46	31.73	0.950082704	0	0.578313253

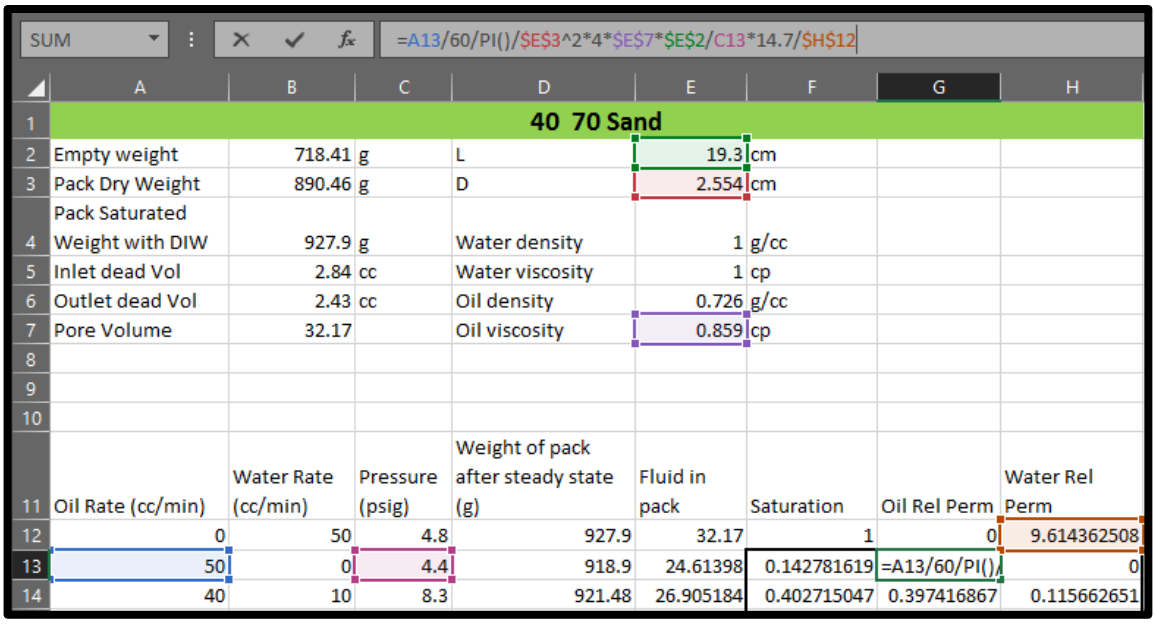
Figure 27: Relative permeability calculations, 1



SUM | =(E13-$B$7*$E$6)/($E$4-$E$6)/$B$7

	A	B	C	D	E	F	G	H
1	40 70 Sand							
2	Empty weight	718.41	g	L	19.3	cm		
3	Pack Dry Weight	890.46	g	D	2.554	cm		
4	Pack Saturated Weight with DIW	927.9	g	Water density	1	g/cc		
5	Inlet dead Vol	2.84	cc	Water viscosity	1	cp		
6	Outlet dead Vol	2.43	cc	Oil density	0.726	g/cc		
7	Pore Volume	32.17		Oil viscosity	0.859	cp		
8								
9								
10								
11	Oil Rate (cc/min)	Water Rate (cc/min)	Pressure (psig)	Weight of pack after steady state (g)	Fluid in pack	Saturation	Oil Rel Perm	Water Rel Perm
12	0	50	4.8	927.9	32.17	1	0	9.614362508
13	50	0	4.4	918.9	24.61398	=(E13-$B$7*$E	0.937090909	0
14	40	10	8.3	921.48	26.905184	0.402715047	0.397416867	0.115662651

Figure 28: Relative permeability calculations, 2



SUM | =A13/60/PI()/$E$3^2*4*$E$7*$E$2/C13*14.7/$H$12

	A	B	C	D	E	F	G	H
1	40 70 Sand							
2	Empty weight	718.41	g	L	19.3	cm		
3	Pack Dry Weight	890.46	g	D	2.554	cm		
4	Pack Saturated Weight with DIW	927.9	g	Water density	1	g/cc		
5	Inlet dead Vol	2.84	cc	Water viscosity	1	cp		
6	Outlet dead Vol	2.43	cc	Oil density	0.726	g/cc		
7	Pore Volume	32.17		Oil viscosity	0.859	cp		
8								
9								
10								
11	Oil Rate (cc/min)	Water Rate (cc/min)	Pressure (psig)	Weight of pack after steady state (g)	Fluid in pack	Saturation	Oil Rel Perm	Water Rel Perm
12	0	50	4.8	927.9	32.17	1	0	9.614362508
13	50	0	4.4	918.9	24.61398	0.142781619	=A13/60/PI()	0
14	40	10	8.3	921.48	26.905184	0.402715047	0.397416867	0.115662651

Figure 29: Relative permeability calculations, 3

Simulation setup

Simulations were run using CMG GEM 2015 simulator. The primary objective was to verify that relative permeability modifications enhance production. Relative permeability data obtained from sand pack flooding experiments was input in a simple model to observe the effect of wettability alteration of proppants.

The reservoir was described as 1010ft x 1010ft x 70ft. Each grid-block was 10ft x 10ft x 10ft. Depth of the reservoir was set at 6000ft (grid top, for layer 1), with a reference pressure of 4500psi. The depth of oil-water contact was set as 6070ft, with an infinite acting aquifer connected below the reservoir. Presence of an aquifer insured pressure maintenance and fluid supply into the reservoir. A 0.15ft radius well in the center of the reservoir (51, 51, 4) was implemented, with perforations in layers 2 through 6 (Top and bottom most layers were left unperforated). A simple planar fracture of half-length 300ft was implemented through layers 2 through 6, using the Hydraulic fracturing module in CMG Builder. Fracture properties were 0.01ft thickness, with an intrinsic permeability of

5000mD, which led to an effective permeability of 25mD. Refinements of grid were set at 9, 9, 7 in i, j, k directions. The hydraulic fracturing module was used, since it provides excellent fracture modelling with low computational times. Another option was to manually refine the grids in fracture zone, and change the properties to match desired fracture properties. This led to nearly a million grid-blocks in the reservoir and simulator equations did not converge, because of grid-blocks in the fracture region being 0.03-inch in thickness. Initial water saturation for the fracture was set at 1, and for the reservoir at 0.4. The hydrocarbon in the model was implemented as 100% Decane, NC10, with an initial saturation of 0.6 throughout the reservoir. The model was run as a Water-oil model, with no free gas. Relative permeability for the fracture zones was set from experimental data obtained for Sand (Case 1) and Resin coated sand (Case 2). Relative permeability for the reservoir was set using correlations built-in builder. Details of all other model initiation properties are mentioned in Table 5.

Table 5: Reservoir properties for simulator

Grid Type				Cartesian			
Porosity Type				Single			
Property	Layer 1	Layer 2	Layer 3	Layer 4	Layer 5	Layer 6	Layer 7
Grid top	6000 ft	6010 ft	6020 ft	6030 ft	6040 ft	6050 ft	6060 ft
Grid thickness	10 ft	10 ft	10 ft	10 ft	10 ft	10 ft	10 ft
Initial water Saturation	Defined separately for different sectors. Fracture at 1, reservoir at 0.4						
Permeability (I, J, K) mD	30, 30, 3	30, 30, 3	30, 30, 3	30, 30, 3	30, 30, 3	30, 30, 3	30, 30, 3
Porosity	0.35	0.35	0.35	0.35	0.35	0.35	0.35
Rock compressibility	1e-6 1/psi at 2500psi						
Reservoir Temperature	185^{o}F						

Relative Permeability tables for the reservoir and fracture are in Table 6 and Table 7. If a property is not mentioned, then it was left at its default setting.

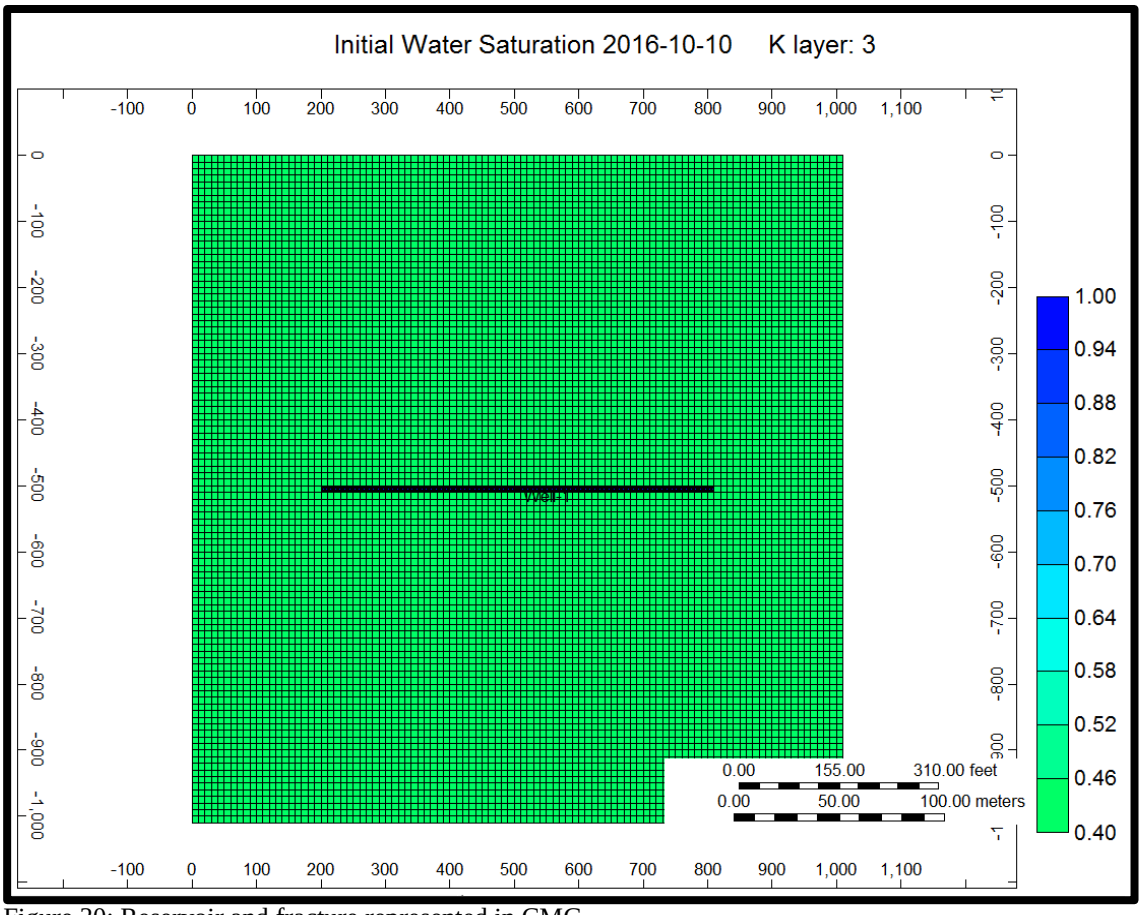


Figure 30: Reservoir and fracture represented in CMG

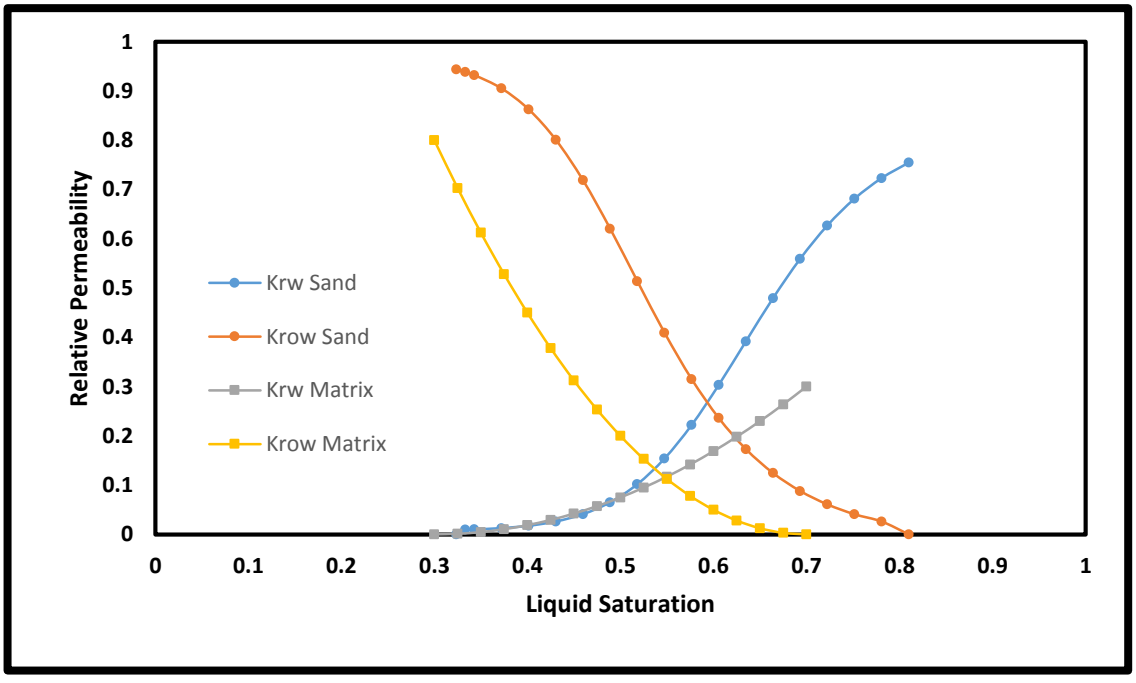


Figure 31: Relative permeability for Case 1 (Sand in fracture zone)

Table 6: Relative permeability tables for reservoir rock

Reservoir Rock Relative Permeability table					
S_w	K_{rw}	K_{row}	SL	K_{rg}	K_{rog}
0.3	0	0.8	0.6	0.8	0
0.325	0.001172	0.703125	0.60625	0.703125	0.003125
0.35	0.004688	0.6125	0.6125	0.6125	0.0125
0.375	0.010547	0.528125	0.61875	0.528125	0.028125
0.4	0.01875	0.45	0.625	0.45	0.05
0.425	0.029297	0.378125	0.63125	0.378125	0.078125
0.45	0.042188	0.3125	0.6375	0.3125	0.1125
0.475	0.057422	0.253125	0.64375	0.253125	0.153125
0.5	0.075	0.2	0.65	0.2	0.2
0.525	0.094922	0.153125	0.65625	0.153125	0.253125
0.55	0.117187	0.1125	0.6625	0.1125	0.3125
0.575	0.141797	0.078125	0.66875	0.078125	0.378125
0.6	0.16875	0.05	0.675	0.05	0.45
0.625	0.198047	0.028125	0.68125	0.028125	0.528125
0.65	0.229687	0.0125	0.6875	0.0125	0.6125
0.675	0.263672	0.003125	0.69375	0.003125	0.703125
0.7	0.3	0	0.7	0	0.8

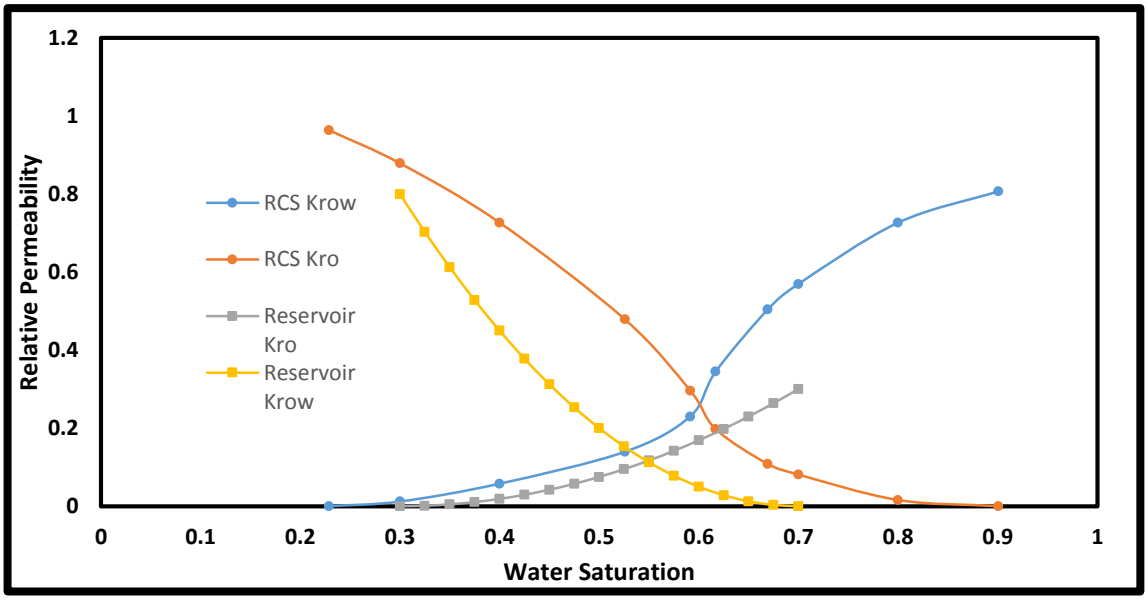


Figure 32: Relative Permeability for Case 2 (Resin Coated Sand in Fracture)

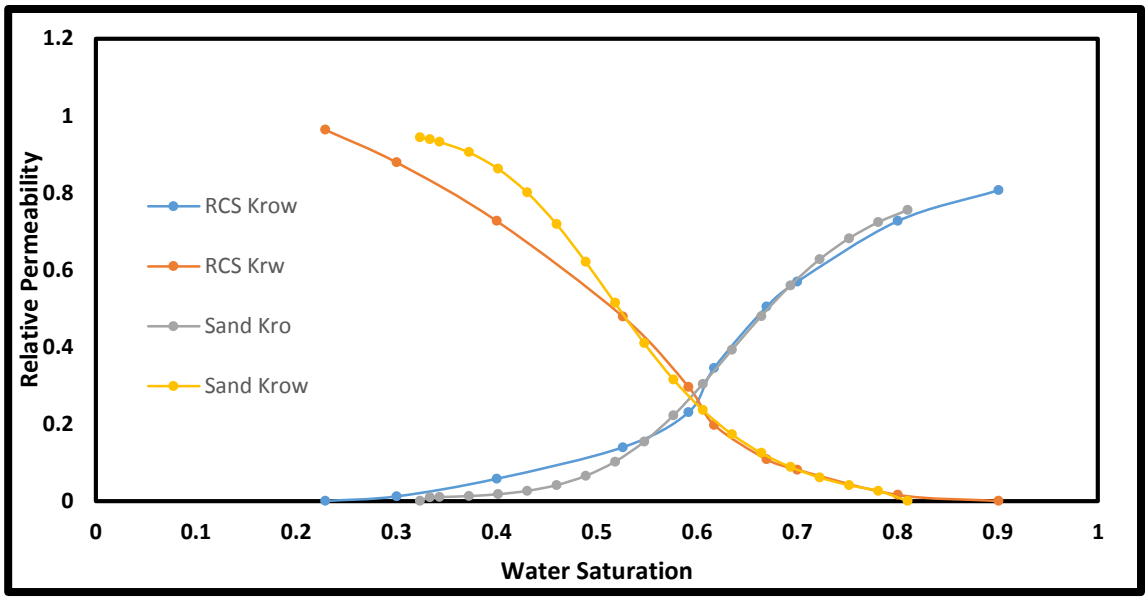


Figure 33: Relative Permeability contrast between Sand and RCS

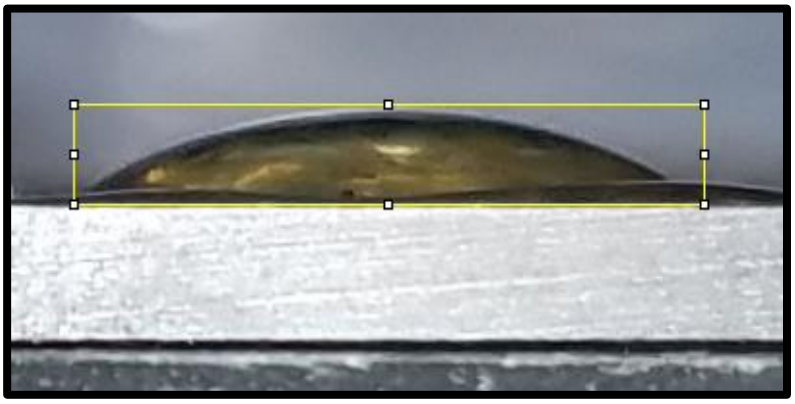
Table 7: Relative permeability tables for the fracture zone (Case 1 and Case 2)

Fracture Relative Permeability table					
Sand Sw	**Sand Krw**	**Sand Krow**	**RCS Sw**	**RCS Krw**	**RCS Krow**
0.323497	0	0.943859	0.228887	0	0.963756
0.333225	0.009691	0.938612	0.3	0.011938	0.879068
0.342953	0.010213	0.932292	0.4	0.057672	0.726976
0.372138	0.012743	0.905276	0.5258	0.139394	0.478958
0.401323	0.017566	0.862687	0.591356	0.23	0.296355
0.430508	0.02627	0.800851	0.616939	0.345	0.19757
0.459693	0.04116	0.71891	0.66917	0.50411	0.108258
0.488878	0.065253	0.620591	0.7	0.569493	0.081096
0.518062	0.101919	0.514103	0.8	0.726676	0.015855
0.547247	0.153938	0.409526	0.900674	0.807018	0
0.576432	0.222024	0.315321			
0.605617	0.303463	0.236182			
0.634802	0.392023	0.173075			
0.663987	0.479716	0.124525			
0.693171	0.559487	0.088014			
0.722356	0.627099	0.060901			
0.751541	0.681366	0.040881			
0.780726	0.723257	0.026109			
0.809911	0.754771	0			

Results and Discussions

Wettability alteration, contact angle results

Contact angle results were one of the primary criterion for treatment selection. The PFDS+TEOS treatment offered excellent primary results on glass slides. The second step was then to check its durability. A treatment capable of good alteration at room temperature and pressure, could possible degrade at higher temperatures, as indicated by the literature review. The selected PFDS+TEOS treatment was found to be durable after immersing it in a water bath at 80^{o}C for over 24hrs. This durability test was sufficient in screening out treatments which would potentially degrade at reservoir temperatures and pressures.



Contact angle of a water droplet on a glass slide was 30^{o}. For a Decane droplet, it was 0^{o}, since it spread out completely on the glass slide.

Figure 34: Untreated glass slide, water-air contact angle.



Figure 35: Water (left, contact angle of 102.6^{o}) and Oil (right, contact angle of 57.5^{o}) droplets on a glass slide with Treatment A (PFDS-1).

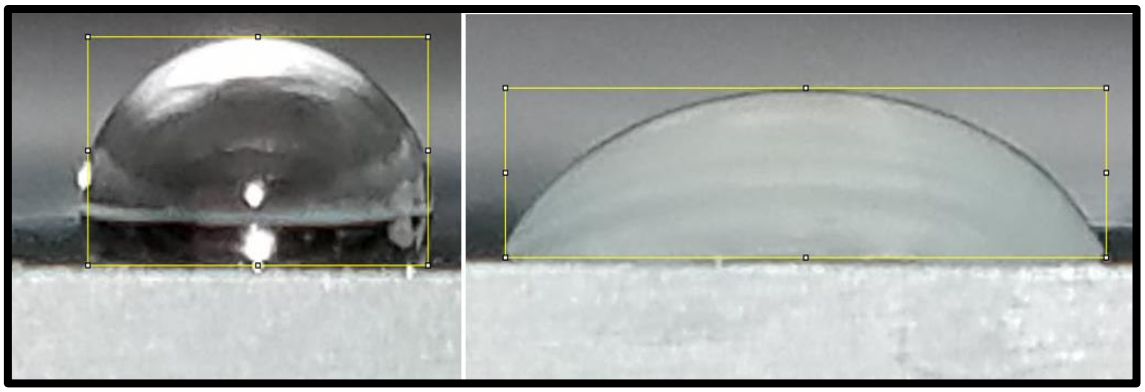


Figure 36: Water (left, contact angle of 103.8º) and Oil (right, contact angle of 56.4º) droplets on a glass slide with Treatment B (PFDS-2).

Contact angle results with treatments A and B, both indicated successful treatment. The degree of alteration was also satisfactory, with results being better than what had been previously reported. Durability tests exhibited insignificant change to water contact angles. This indicated strong bonding of chemicals with the silica substrate of glass.

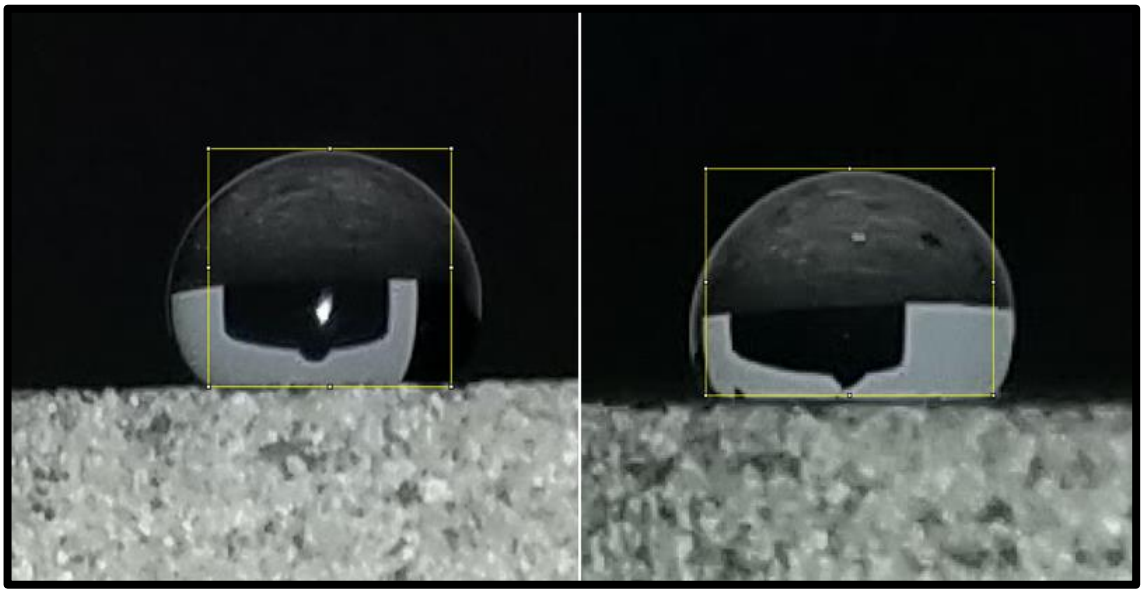


Figure 37: GB1 and GB2 treated with PFDS-1 and PFDS-2 respectively. Water-air contact angle are 123.6º and 112º respectively.

Significant change in results was observed with Decane, but imbibition study results established that it was more of a surface effect. The treatments were carried out with rock samples taken from the same 12-inch core sample, to minimize the differences between rock samples.

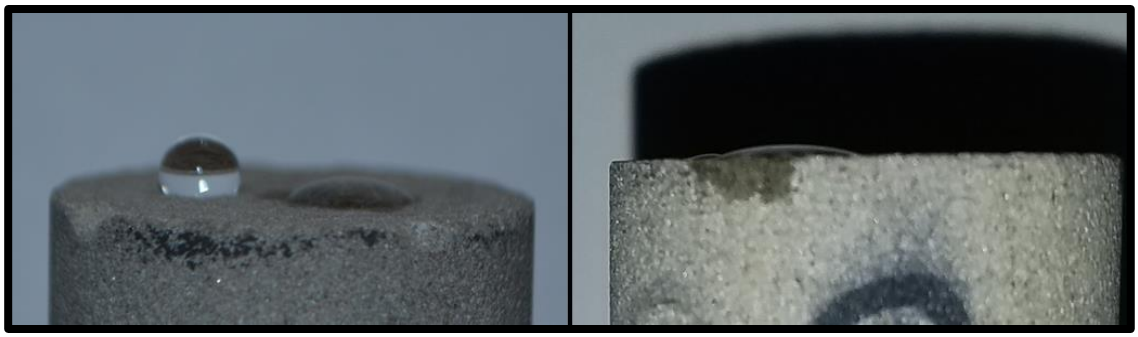


Figure 38: GB1 and GB2 treated with PFDS-1 and PFDS-2 respectively. Decane-air Contact angles, 39^0 and 20^0 respectively.

PFDS-2 was slightly less effective with Decane-air contact angle, but it was still preferred, since it did not result in a permeability reduction.

Wettability Alteration, permeability results

The first permeability tests were done with virgin samples, followed by tests with treated samples. Treatment A (PFDS-1) was abandoned, once it was clear that it resulted in permeability reduction of over 25%. Ergo, rocks were later treated only with treatment B (PFDS-2).

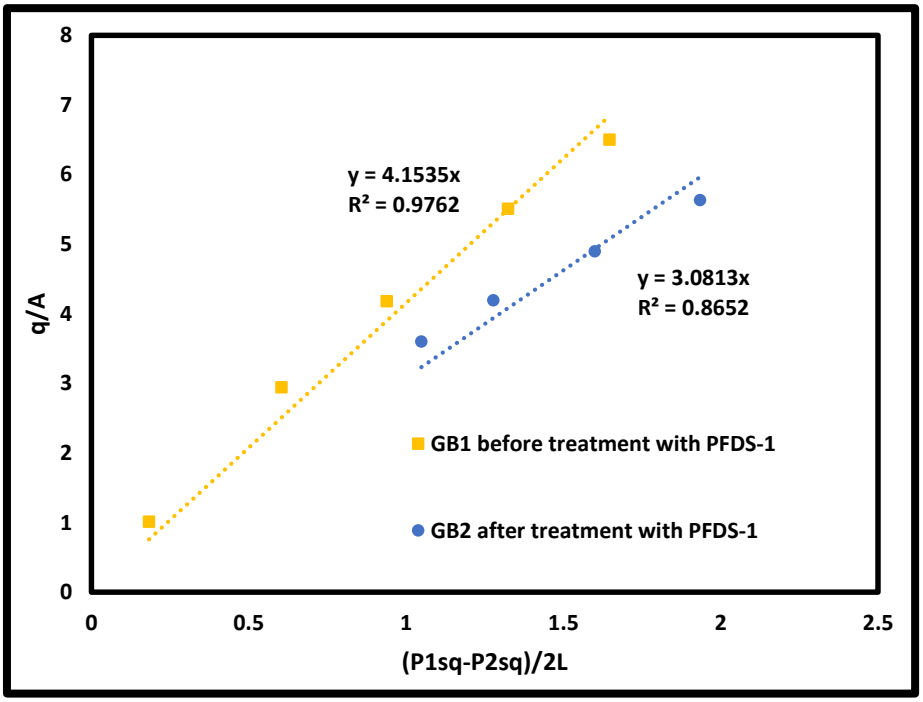


Figure 39: Permeability contrast, before and after treatment, PFDS-1

Figure 39 depicts permeability study done on GB1, a sandstone sample. Difference in base permeability values of GB1 and GB2 is expected, because they were taken from different positions in the same core sample. Permeability before treatment was 74mD, as calculated from the gas-Darcy equation. Permeability after treatment was 55mD, a decrease of 26%. Such results were unacceptable, because commercially any treatment that reduces permeability over 25% becomes challenging to pitch. The reason for permeability reduction was investigated, and it was observed that excess polymer coating was blocking the pores. Treatment of glass slides showed a white powder like residue in some regions. It was theorized, that this excess polymer was responsible for permeability reduction. Figure 40 has 4 pictures of a glass slide, treated with PFDS-1. The right most picture is of residue leftover after gently wiping off the polymer.

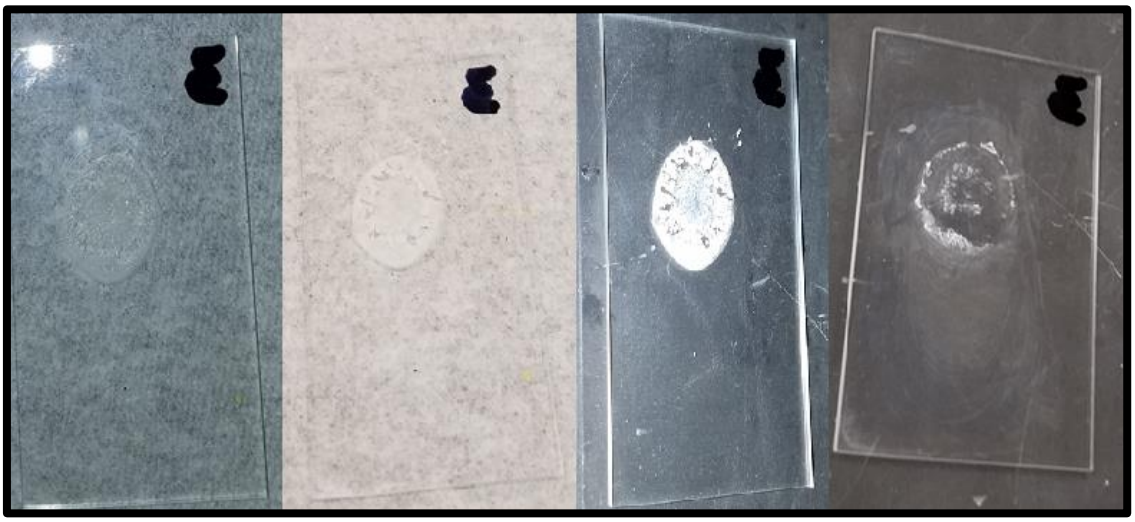


Figure 40: Polymer residue on a glass slide treated with PFDS-1

Figure 41 depicts permeability contrast before and after treatment with PFDS-2 for a sandstone sample. Permeability of 109mD before treatment and 98mD after treatment was observed. A 10% reduction in permeability was deemed acceptable.

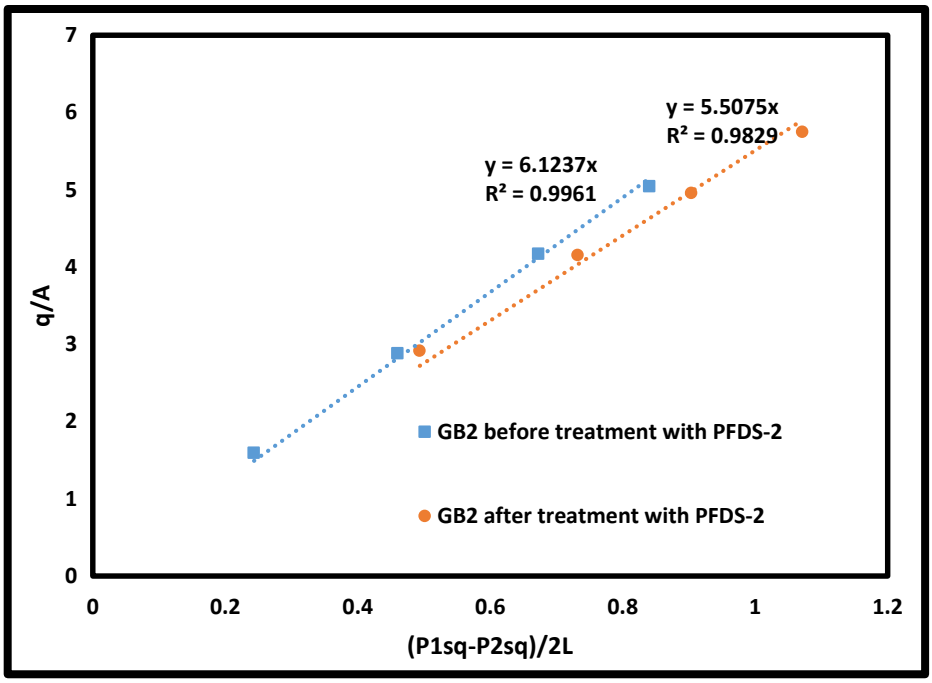


Figure 41: Permeability contrast, before and after treatment, PFDS-2

With successful treatment of sandstone samples, Treatment B (PFDS-2) was tested on limestone samples.

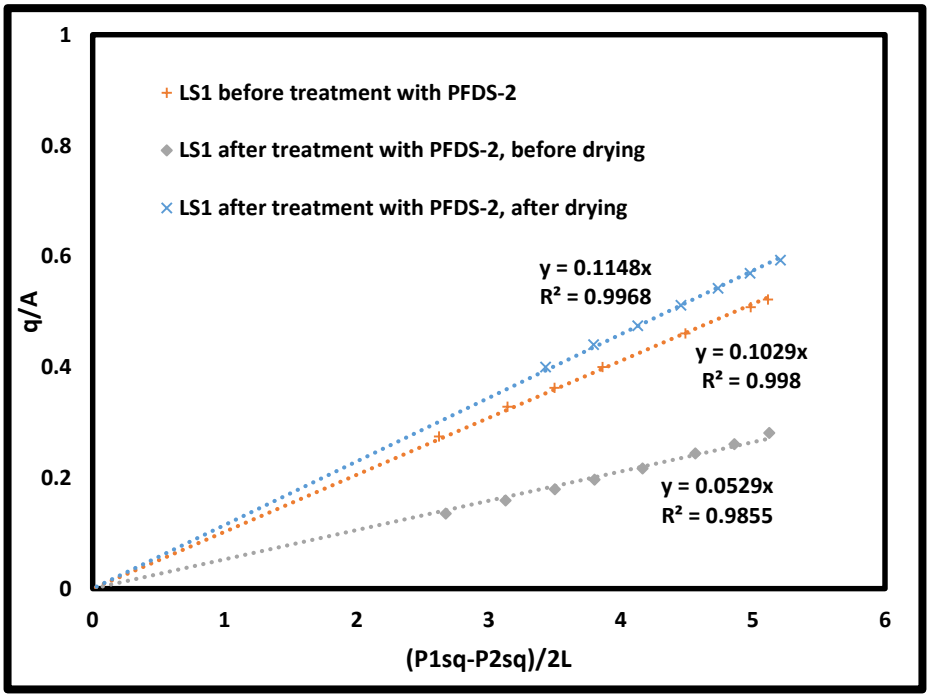


Figure 42: LS1 Permeability test results with PFDS-2 treatment.

Treatment with PFDS-2 for limestone samples exhibited an increase in permeability.

Since the treatment fluid contained acid as a catalyst, it was theorized that the acid was responsible for the increase in permeability of limestone. Figure 42 and Figure 43 show permeability contrast for samples LS1 (1.83mD before treatment, 0.94mD after treatment but before drying and 2.04mD after treatment and drying) and LS2 (2.43mD before treatment and 3.48mD after treatment) treated with PFDS-2. The first treatment of LS1 exhibited an increase in permeability, ergo to verify that the result was not anomalous, a second sample was treated. The LS3 sample again exhibited an increase in permeability. Further it was observed, that permeability of limestone initially reduced after treatment, but once the sample was heated to 80^{o}C and allowed to cool, its permeability rebounded. Low permeability limestone most probably did not allow for proper cleanup of the treatment fluid with just air flow. Heating in the oven at 80^{o}C evaporated away any

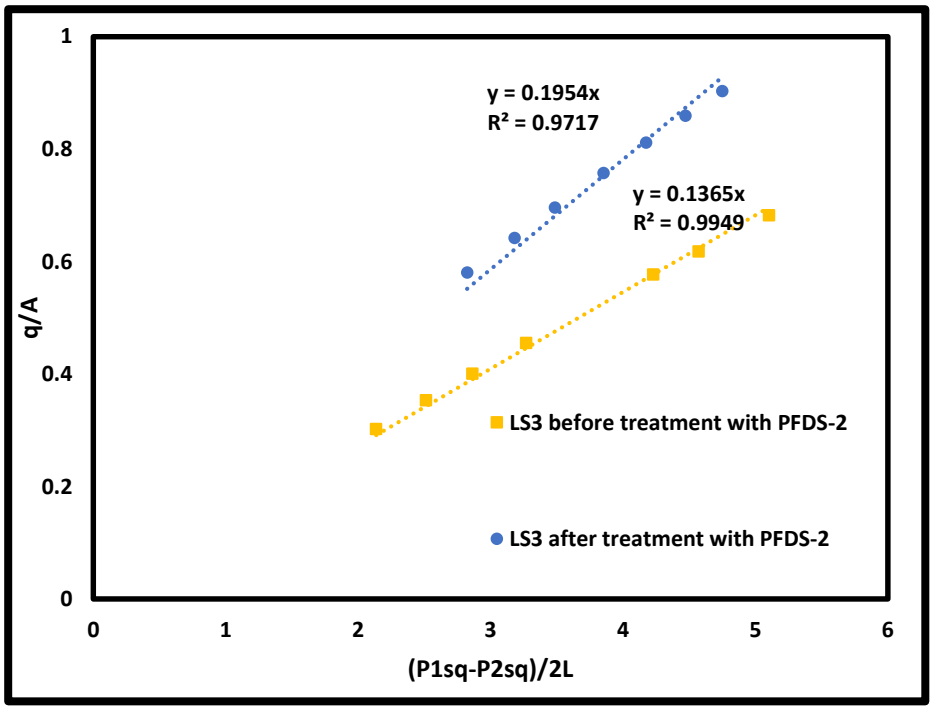


Figure 43: LS3 permeability contrast with PFDS-2 treatment.

residual fluid. Reservoir temperatures are usually higher than 80^{o}, thus it was concluded that the treatment procedure was viable.

Wettability Alteration, imbibition results

Spontaneous imbibition studies at room temperature and pressure were conducted to observe the results of wettability alteration treatment.

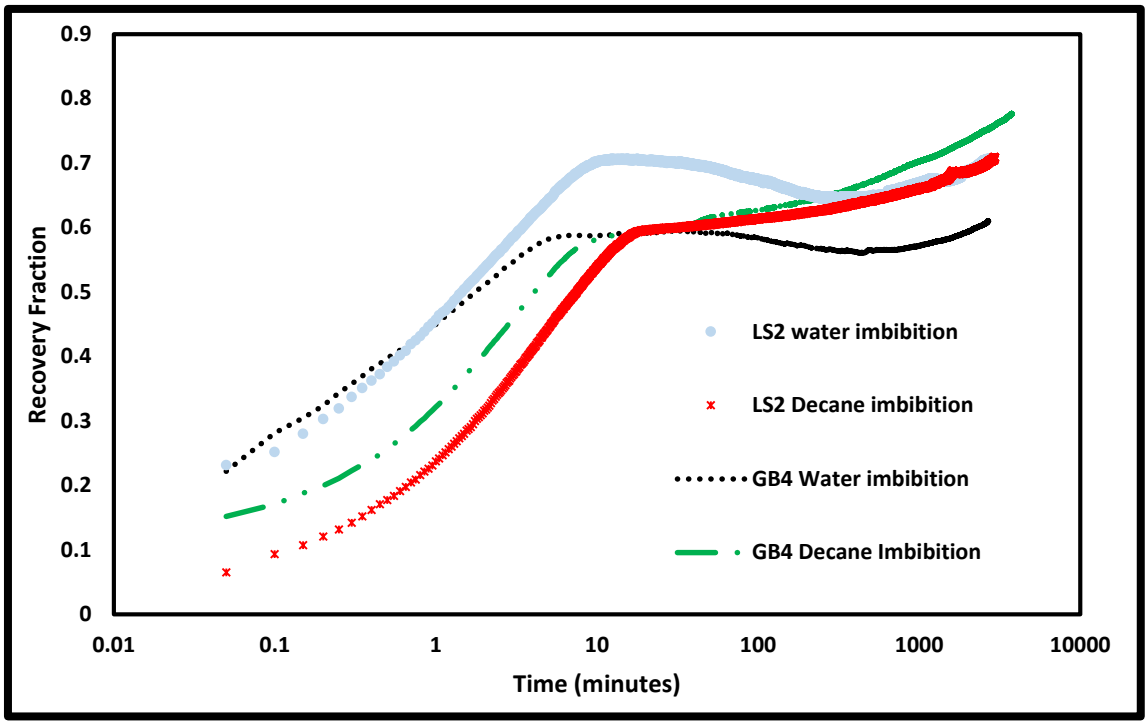


Figure 44: Imbibition in reference rocks (untreated rocks)

Spontaneous imbibition experiments were started with fresh, clean cut samples, on which porosity and permeability measurements had been conducted. The final water saturations were at 61% for GB4 and 70.5% for LS2, while the Decane saturations were calculated at 77.5% for GB4 and 70.7% for LS2. These numbers represent saturation values, when an air saturated (dry) core was immersed in the respective fluid. Another aspect of initial saturation was the order of actions. A fresh sample that went through water imbibition followed by a Decane imbibition (after drying and cooling), would exhibit a hysteresis effect. The shape of the curves was similar, but the final saturations differed. This was observed in Figure 45.

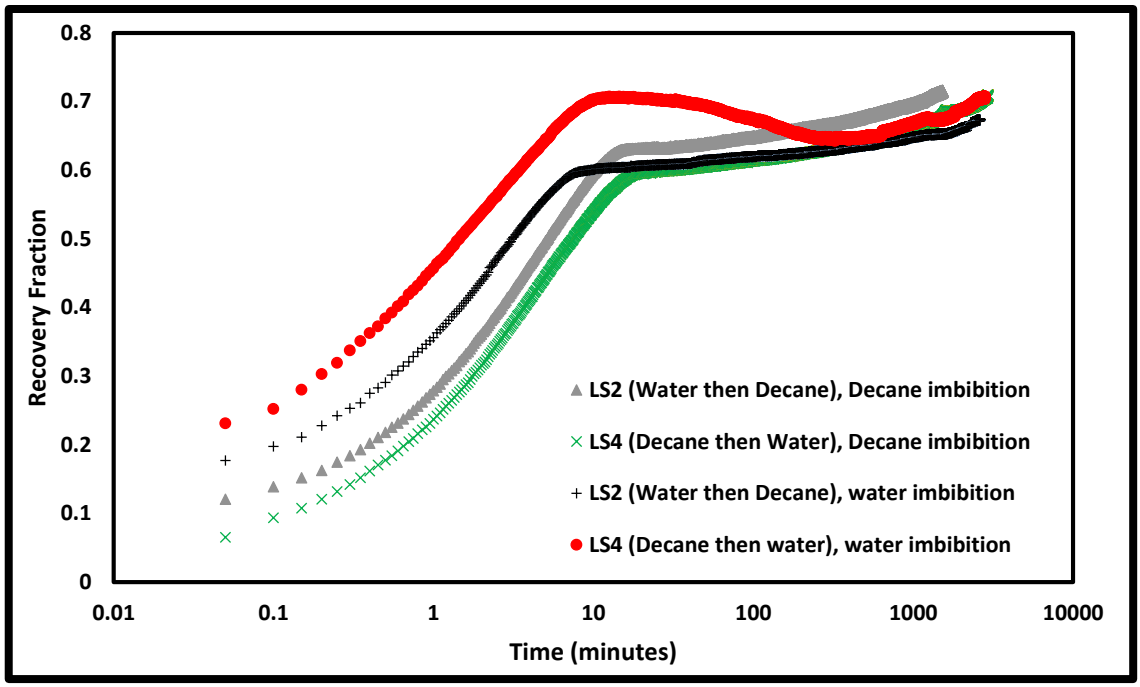


Figure 45: Hysteresis effect of imbibition in different samples (untreated)

The characteristic 'hump' observed in all water imbibition experiments is a common



Figure 46: Air bubbles sticking to rock surface during water imbibition.

feature. It can be explained by the physical properties of water, and its interaction with the rock surface. The surface energy of leaving water bubbles is such that, it sticks around on the surface of rocks for a while. The buoyancy provided by those air bubbles decreases

the weight on string (ergo lower recovery fraction observed). Once the bubbles leave, the recovery fraction goes back to normal. The properties of Decane preclude the occurrence of this effect with Decane-air imbibition experiments. This effect can be better understood with the picture in Figure 46.

Figure 47 represents water and Decane imbibition in Indiana Limestone samples. It can be inferred that PFDS-1 was the most successful treatment, with a water recovery fraction

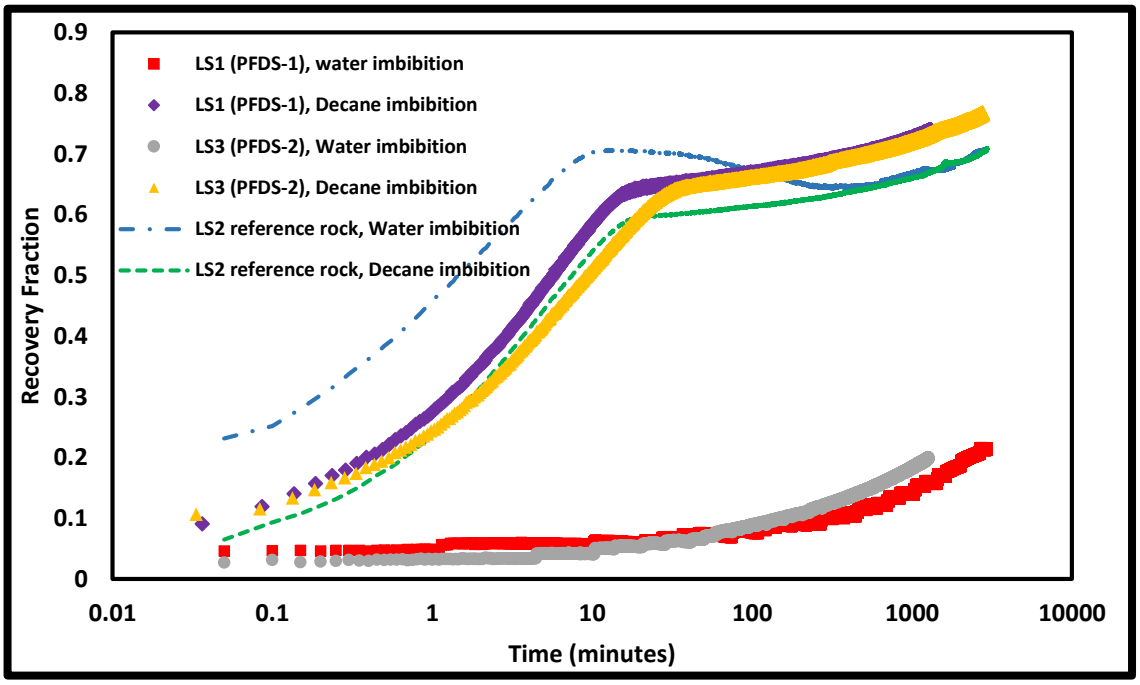


Figure 47: Water and Decane imbibition in Limestone

at 0.213 and Decane recovery at 0.71. PFDS-2 was also a successful treatment, with final water recovery fraction 0.20 and Decane recovery at 0.77. Decane recoveries for both PFDS-1 and PFDS-2 were slightly higher than the reference case, this slight negative effect though was compensated by the huge gain in water mobility. It is expected, with

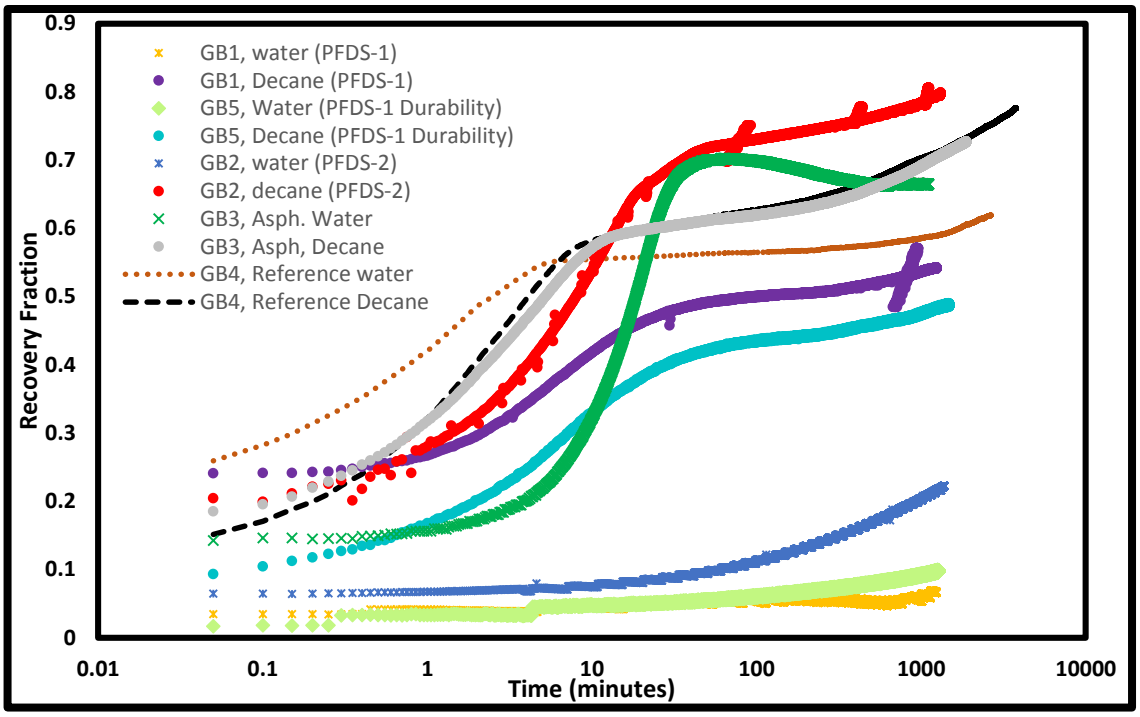


Figure 48: Water and Decane imbibition in Sandstone

this treatment, water blockage in limestone reservoirs can be resolved on a permanent basis.

Figure 48 represents water and Decane imbibition in Grey Berea samples. It can be inferred that PFDS-1 was the most successful treatment, with a water recovery fraction at 0.213 and Decane recovery at 0.71. PFDS-2 was also a successful treatment, with final water recovery fraction 0.20 and Decane recovery at 0.77. Decane recoveries for both PFDS-1 and PFDS-2 were slightly higher than the reference case, this slight negative effect though was compensated by the huge gain in water mobility. It is expected, with this treatment,

Figure 48 represents water and Decane imbibition in Grey Berea samples. It can be inferred that PFDS-1 was the most successful treatment, with a water recovery fraction at 0.06 and Decane recovery at 0.54. exceptional performance can be attributed to both

polymerization of the treatment and strong bonding with the silica substrate. The durability of the treatment, is one more indicator of strong bond formation between the treatment and the rock surface. PFDS-2 was also a successful treatment, with final water recovery fraction 0.22 and Decane recovery at 0.78. Decane recoveries for PFDS-1 was less than reference rock, indicating excellent performance for both water and Decane. For PFDS-2, water performance was excellent, but Decane recovery was slightly higher than reference rock (0.78 for PFDS-2 and 0.77 for reference rock). Though PFDS-2 does not perform as well as PFDS-1 in terms of Decane recovery, the gain from higher water mobility more than compensates for it. Another factor that could be giving better results for PFDS-1 recovery is the reduction in permeability it causes. Thus, Treatment B, PFDS-2 was selected as the most viable treatment from this study.

GB3 sample represents a sample, through which Texas Crude was forced to flow. This resulted in Asphaltene deposition in the rock. In tandem with reduction in permeability, it was observed that Asphaltene deposition alters the wettability state of the rock slightly. Deposition of Asphaltene did not alter oil mobility, but it did reduce water mobility. This is an expected result, since Asphaltene and water are immiscible, and Asphaltene viscosity is several orders of magnitude higher than water.

Proppant Pack Flooding, Permeability, and Relative permeability

The first results with proppant packs were the porosity and permeability results. Introduced in the theoretical background section, proppant packs exhibited non-Darcy flow behavior. Figure 9 (Darcy flow for 8x12 proppant) and Figure 10 (non-Darcy flow for 8x12, 12x20 and 16x20 proppants) depict Darcy and non-Darcy flow plots for some of the tested proppants. Proppants with very high permeability values (76 Darcy for 8x12, 106 Darcy for 12x20, 104 Darcy for 16x20) were not investigated further.

Smaller proppants selected for tests were 40x70 US mesh size distribution Sand (referred to as sand) (Primarily water wet), and 50x80 Resin Coated Sand (abbreviated as RCS) (Primarily neutral/oil wet). Absolute water permeability values for these proppant packs were very similar, 9 Darcy for Sand, and 9.5 Darcy for RCS. Porosity values for both were at 28.5% porosity. These values were consistent, and had very little variation throughout several packing runs. This indicated that the proppant packing methodology used was effective and consistent.

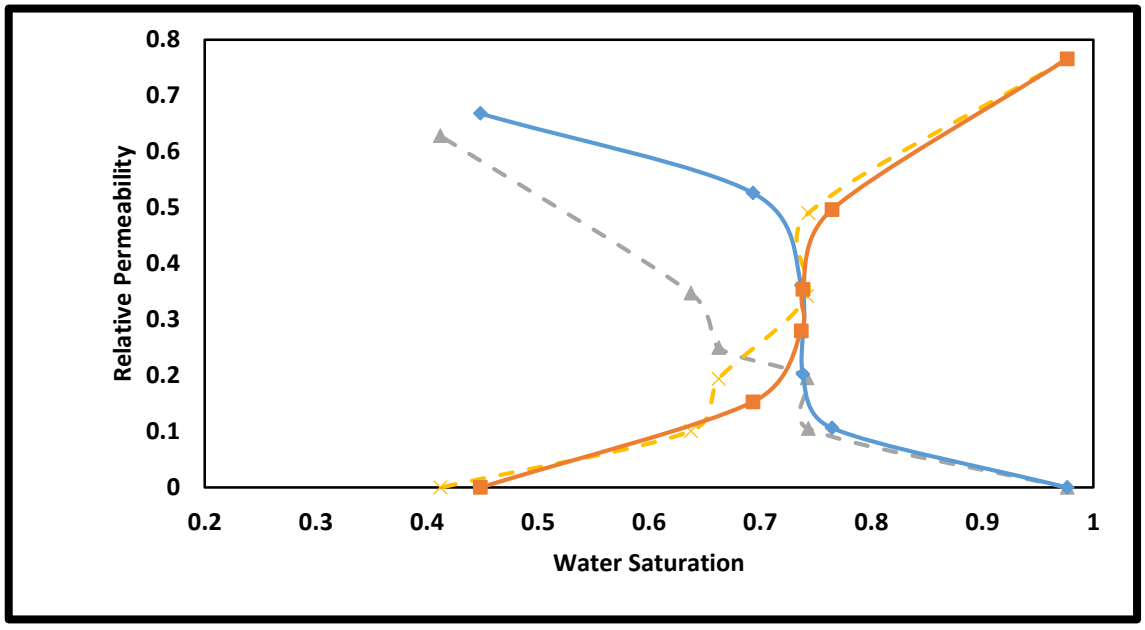


Figure 49: Relative Permeability curves for oil-water, 40x70 Sand

Figure 49 depicts relative permeability curves obtained for 40x70 Sand at 50cc/min flow-rate. The solid line curves are for an initially 100% water saturated pack, which was progressively drained. The dashed lines depict hysteresis in the pack. Similar end-points and shape of data reaffirm the experimental methodology. Table 8 contains the calculated relative permeability data. The rate data as represented, was how the experiment was conducted. Thus, initial water rate was used to determine Darcy permeability, followed by the combinations.

Table 8: Relative permeability table for Oil-water, 40x70 Sand. Absolute water permeability 8.98 Darcy.

Oil Rate (cc/min)	Water Rate (cc/min)	Water Saturation	Oil Relative Permeability	Water Relative Permeability
0	50	1	0	1
50	0	0.447968543	0.668111111	0
40	10	0.693408853	0.5261375	0.153125
30	20	0.736917557	0.36078	0.28
20	30	0.738305558	0.202848193	0.354216867
10	40	0.764470444	0.106559494	0.496202532
0	50	0.97646196	0	0.765625
0	50	0.97646196	0	0.765625
10	40	0.743410092	0.1052275	0.49
20	30	0.742022091	0.195772093	0.341860465
30	20	0.662586905	0.250045545	0.194059406
40	10	0.637660864	0.347142268	0.101030928
50	0	0.412042061	0.628223881	0

Like Figure 49, Figure 50 represents relative permeability plots for RCS at 500cc/min. The solid line curves are for an initially 100% water saturated pack, which was progressively drained. The dashed lines depict hysteresis in the pack. Similar end-points and shape of data reaffirm the experimental methodology. Table 9 contains the calculated relative permeability data. The rate data as represented, was how the experiment was

conducted. Thus, initial water rate was used to determine Darcy permeability, followed by the combinations.

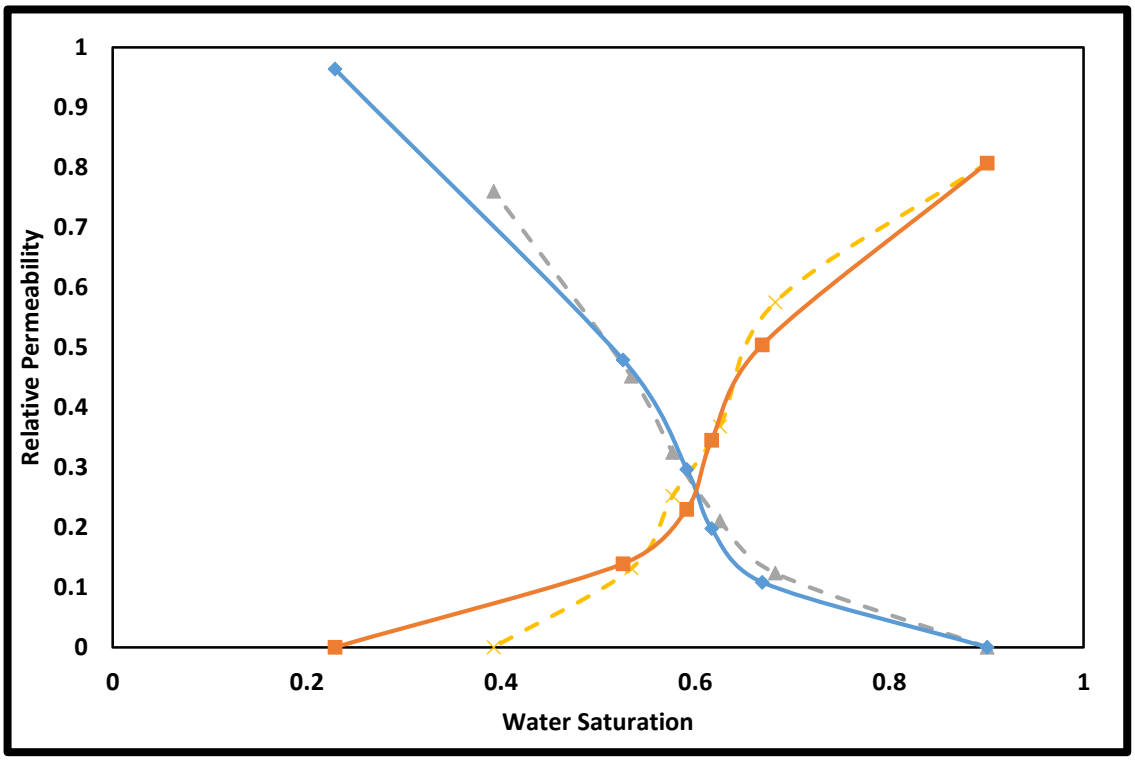


Figure 50: Relative Permeability curves for oil-water, 50x80 RCS

Table 9: Relative permeability table for Oil-water, 50x80 RCS. Absolute water permeability 9.46 Darcy

Oil Rate (cc/min)	Water Rate (cc/min)	Water Saturation	Oil Relative Permeability	Water Relative Permeability
0	50	1	0	1
50	0	0.228886504	0.963756098	0
40	10	0.525799879	0.478957576	0.139393939
30	20	0.591355707	0.296355	0.23
20	30	0.616938764	0.19757	0.345
10	40	0.669170335	0.108257534	0.504109589
0	50	0.900673723	0	0.807017544
0	50	0.900673723	0	0.807017544
10	40	0.682494592	0.12348125	0.575
20	30	0.625417837	0.210741333	0.368
30	20	0.576820154	0.324772603	0.252054795
40	10	0.534278952	0.451588571	0.131428571
50	0	0.392411472	0.759884615	0

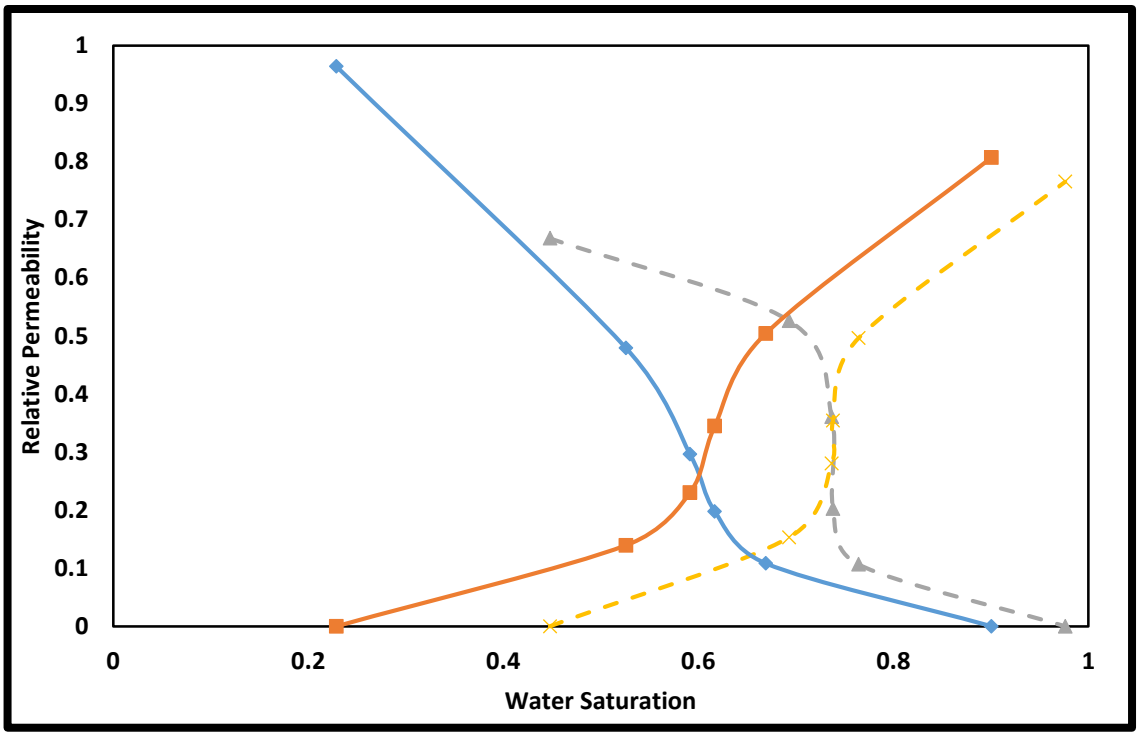


Figure 51: Relative permeability comparison between RCS (Solid lines) and Sand (Dashed lines)

Comparative study of relative permeability curves of Sand and RCS reveals expected results. Water wet sand has better mobility for water, with a higher irreducible water saturation. Oil/Neutral wet RCS has better oil mobility, with a much lower irreducible water saturation.

Note that these curves were developed with the assumption of Darcy flow in proppant pack. With several experiments, it was found that deviation from Darcy flow starts at approximately 40cc/min net flow rate for the setup used here. Thus, the assumed Darcy flow is expected to give fairly accurate results. To investigate the non-Darcy flow behavior, and relative permeability developed with non-Darcy flow, the experiments were conducted again at 50cc/min and 100cc/min. and data was fitted to the Forchheimer equation. Literature review on non-Darcy flow relative permeability was found to be lacking, and this area of the study was recommended for further investigation. Figure 51

and Figure 53 depict the calculated relative permeability curves for RCS and Sand at 50cc/min and 100cc/min. the curves for a derived average between 50cc/min and 100cc/min are also present.

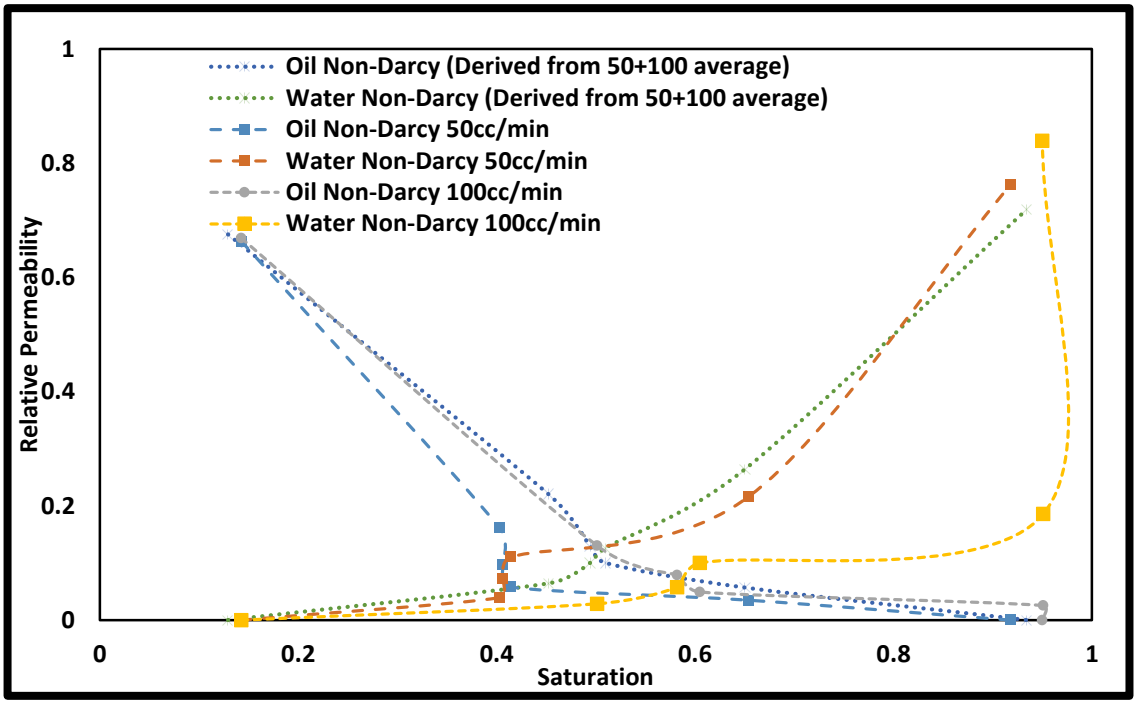


Figure 52: Non-Darcy relative permeability for RCS.

Table 10: Non-Darcy relative permeability table for RCS. Absolute water permeability 28.7 Darcy.

Oil Rate (cc/min)	Water Rate (cc/min)	Water Saturation	Oil Relative Permeability	Water Relative Permeability
0	50	1	0	1
50	0	0.142781619	0.663269195	0
40	10	0.402715047	0.162114185	0.039356064
30	20	0.406255091	0.096762016	0.072363499
20	30	0.414333071	0.057985909	0.110261562
10	40	0.653845787	0.034939912	0.215960265
0	50	0.918317152	0	0.762825557
0	50	0.142781619	0.668818589	0
10	40	0.501415155	0.130261467	0.028730735
20	30	0.582100111	0.078700801	0.057543938
30	20	0.604926383	0.049298553	0.099969411
40	10	0.951080596	0.025546967	0.186063245
50	0	0.950082704	0	0.839194282

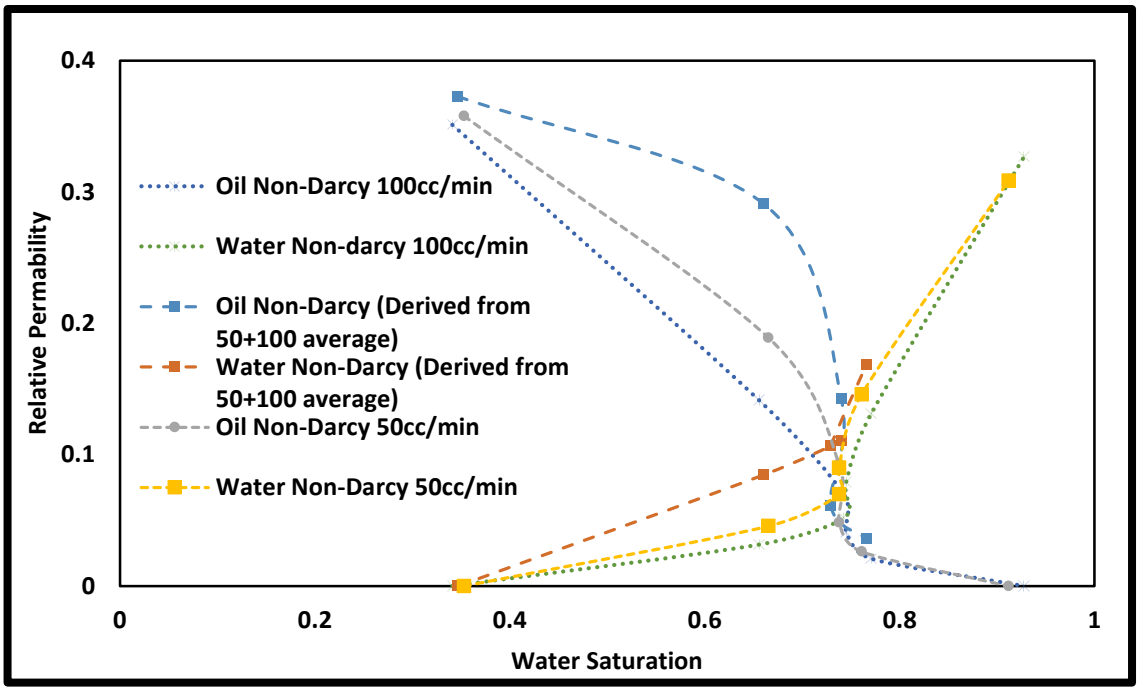


Figure 53: Non-Darcy relative permeability for Sand.

Table 11: Non-Darcy relative permeability table for Sand. Absolute water permeability 25.42 Darcy.

Oil Rate (cc/min)	Water Rate (cc/min)	Water Saturation	Oil Relative Permeability	Water Relative Permeability
0	50	1	0	1
50	0	0.353022313	0.357773272	0
40	10	0.665442164	0.188995592	0.045635673
30	20	0.737928956	0.092953214	0.06989457
20	30	0.738074121	0.048443937	0.090034803
10	40	0.761127468	0.026203369	0.145921362
0	50	0.911984355	0	0.308566723
0	50	0.340965375	0.351153831	0
10	40	0.655796614	0.14142919	0.031486571
20	30	0.742751731	0.069804032	0.051680333
30	20	0.745308284	0.040711605	0.079128912
40	10	0.770773019	0.020804642	0.130937941
50	0	0.927658374	0	0.32648382

This data and the associated non-Darcy calculations have been theorized. Literature does not back calculations for non-Darcy relative permeability. These were presented here

with the view, that further work needs to be done on these. A trend was noticed, while averaging data for 50cc/min and 100cc/min flowrates. It's depicted in Figure 54 and Figure 55.

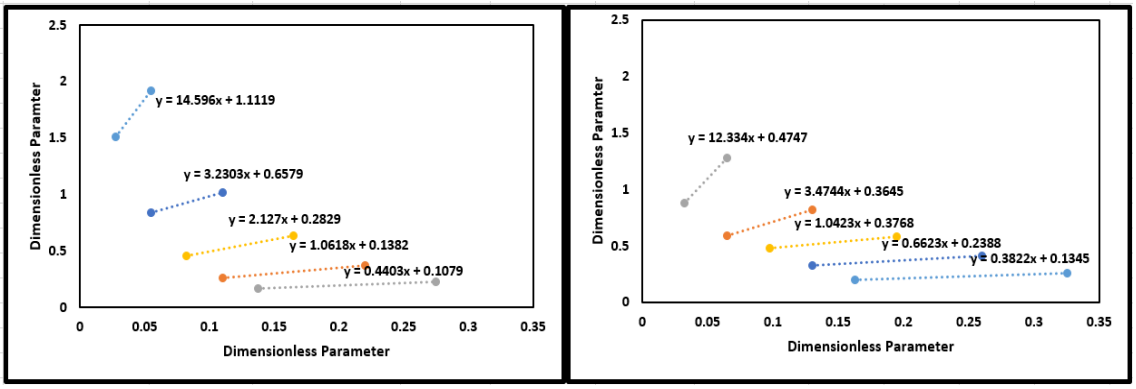


Figure 54: Non-Darcy Forchheimer equation between 50cc/min and 100cc/min flowrates for Oil(Left) and Water(Right) in Sand.

The trend was developed using the average saturation for the two rates. First an average value of saturation was calculated. Next, the flow rates of 50cc/min and 100cc/min were plotted on Forchheimer equation (as done for previous permeability calculations), for each rate combination. Thus Figure 54 represents rate sets of 50 & 100cc/min water ($y = 0.3822x + 0.1345$), 40 & 80cc/min water ($y = 0.6623x + 0.2388$) and so on as represented in Table 12**.** A plot of ρ.Q/μ.A vs ($P1-P2$)A/(μ.L.Q) for all the data in Table 12 would generate Figure 54. It's expected that further investigation of this would possibly clarify relative permeability curve generation in presence of non-Darcy flow. Similarly, Figure 55 for RCS can be generated by data in Table 13.

Table 12: Sand relative permeability data, Forchheimer calculations

Oil Rate (cc/min)	Water Rate (cc/min)	ρ.Q/ μ.A	($P1-P2$) A/(μ.L.Q)	K_e	K_{ro}	ρ.Q/μ. A	($P1-P2$)A /(μ.L.Q)	K_e	K_{rw}
0	50					0.162662367	0.108508832	25.416323	1
50	0	0.137477	0.168427	9.093281	0.357773	0.000000	0.000000	0.000000	0.000000
100	0	0.274954	0.228955	8.925039	0.351154	0.000000	0.000000	0.000000	0.000000
40	10	0.109982	0.254943	4.803573	0.188996	0.032532	0.875983	1.159891	0.045636
80	20	0.219963	0.371723	3.594610	0.141429	0.065065	1.277239	0.800273	0.031487
30	20	0.082486	0.458348	2.362529	0.092953	0.065065	0.590582	1.776463	0.069895
60	40	0.164973	0.633793	1.774162	0.069804	0.130130	0.816642	1.313524	0.051680
20	30	0.054991	0.835554	1.231267	0.048444	0.097597	0.478494	2.288354	0.090035
40	60	0.109982	1.013191	1.034739	0.040712	0.195195	0.580221	2.011166	0.079129
10	40	0.027495	1.513208	0.665993	0.026203	0.130130	0.324961	3.708785	0.145921
20	80	0.054991	1.914537	0.528778	0.020805	0.260260	0.411147	3.327961	0.130938
0	50	0.000000	0.000000	0.000000	0.000000	0.162662	0.196672	7.842632	0.308567
0	100	0.000000	0.000000	0.000000	0.000000	0.325325	0.258839	8.298018	0.326484

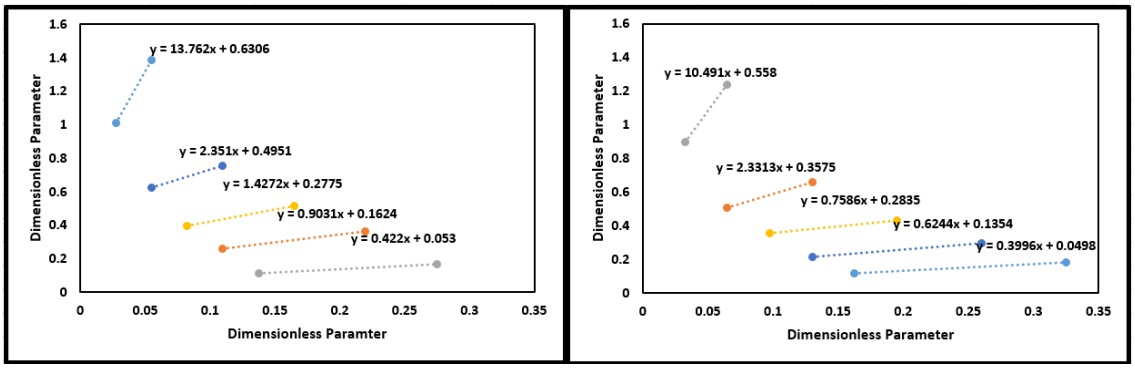


Figure 55: Non-Darcy Forchheimer equation between 50cc/min and 100cc/min flowrates for Oil(Left) and Water(Right) in RCS.

Table 13: RCS relative permeability data, Forchheimer calculations

Oil Rate (cc/min)	Water Rate (cc/min)	ρ.Q/ μ.A	($P1-P2$)A/(μ.L.Q)	K_e	K_{ro}	ρ.Q/μ.A	($P1-P2$)A/(μ.L.Q)	K_e	K_{rw}
0	50					0.162662367	0.097510365	35.27793922	
50	0	0.137477	0.110994	19.033743	0.539537	0.000000	0.000000	0.000000	0.000000
100	0	0.274954	0.169013	19.192993	0.544051	0.000000	0.000000	0.000000	0.000000
40	10	0.109982	0.261718	4.652168	0.131872	0.032532	0.899262	1.129395	0.032014
80	20	0.219963	0.361044	3.738095	0.105961	0.065065	1.240549	0.824482	0.023371
30	20	0.082486	0.395204	2.776766	0.078711	0.065065	0.509221	2.076605	0.058864
60	40	0.164973	0.512925	2.258466	0.064019	0.130130	0.660904	1.651330	0.046809
20	30	0.054991	0.624339	1.664014	0.047169	0.097597	0.357538	3.164161	0.089692
40	60	0.109982	0.753621	1.414714	0.040102	0.195195	0.431574	2.868808	0.081320
10	40	0.027495	1.009032	1.002666	0.028422	0.130130	0.216690	6.197382	0.175673
20	80	0.054991	1.387420	0.733118	0.020781	0.260260	0.297948	5.339431	0.151353
0	50	0.000000	0.000000	0.000000	0.000000	0.162662	0.114846	21.890698	0.620521
0	100	0.000000	0.000000	0.000000	0.000000	0.325325	0.179852	24.082241	0.682643

Simulation results

Results of water and oil production, for 2 different cases were compared, to prove that wettability alteration of the proppant in fracture can improve production.

Table 14: Simulation run summary

	Maximum Bottom Hole Fluid rate	Minimum Bottom Hole Pressure	Fracture zone, Relative Permeability
Case 1	5000 bbl/day	2000 psi	Sand
Case 2	5000 bbl/day	2000 psi	Resin Coated Sand

The simulations were run with a constraint of minimum bottom hole pressure and a maximum bottom hole fluid rate. As theorized, modification of the relative permeability in fracture zone resulted in lower water production (10% lower), and higher oil production rates (5% higher). The relative permeability used here was for resin coated sand, relative permeability for treated sand would exhibit even better results, because of the higher oil mobility. This was only a proof of concept, where all the parameters were the same, and only the relative permeability between two cases was changed in the input data file.

Cost Analysis

A basic cost analysis of the treatment was done. It showed the cost of treatment for a 20ft region around a 10ft long wellbore as $247000. This can be easily deemed feasible for benefits reaped from such a treatment. Similarly, for a proppant pack, the cost was calculated as $16000, again a feasible number. Details of calculation breakdown are in Table 15.

Table 15: Cost Analysis for treatment

Wellbore	USD	Fracture	USD
Radius (ft)	10	Fracture Width (inch)	0.2
Height (ft)	30	Fracture height (ft)	70
Porosity	0.35	Fracture Half Length (ft)	300
Total Vol (ft3)	3298.672	Porosity	0.3
Total Vol to be treated (Bbl)	587.5186	Total Vol to be treated (ft3)	210
PFDS required (at 1 wt%) (kg)	747.264	PFDS required (at 1 wt%) (kg)	47.5723
Per kg Cost ($)	300	Total Vol (Bbl)	37.4026
Cost of PFDS ($)	224179.2	Per kg Cost ($)	300
Cost of other components ($)	22417.92	Cost of PFDS ($)	14271.69
Total Cost of treatemt fluid ($)	246597.1	Cost of other components ($)	1427.169
		Total Cost of treatemt fluid ($)	15698.86

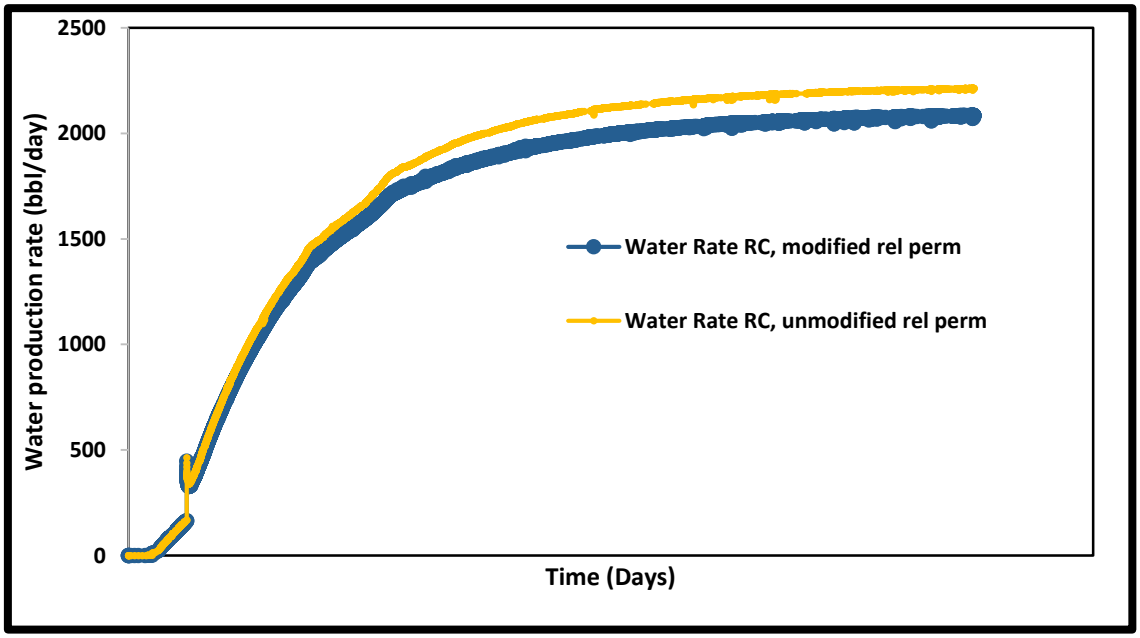


Figure 56: Simulated water production rates (Reservoir Conditions)

Scope for continued research

With the results obtained in this work, several avenues of further research look interesting.

1. Molecular study of the treatment chemicals and their bonding mechanisms would further help in implementing treatments. Images of structured nano-Silica particles on the rock surface would help in optimizing treatment efficiency.

2. Forchheimer equation has been shown to overestimate permeability, implementation of the Barre and Conway equations for characterizing non-Darcy flow could offer better insights.
3. Study of molecular interactions between treatment chemicals, salts and rock surfaces could increase the efficiency (Polymerization efficiency) and durability of the treatment even further. In-depth study of the durability of this treatment would allow its implementation in heavy oil reservoirs
4. Non-Darcy flow behavior and its effect on relative permeability of proppant packs is something that needs to be explored further.
5. Better simulation models, with gas-condensate reservoir fluid and relative permeability from treatment of sand with PFDS would aid in estimating incremental gains from this treatment.
6. With a cost analysis, field scale implementation, study and eventual commercialization of this treatment method is likely.

References

Adibhatla, B., Mohanty, K. K., Berger, P., & Lee, C. (2006). Effect of surfactants on wettability of near-wellbore regions of gas reservoirs. *Journal of Petroleum Science and Engineering, 52*(1–4), 227-236. doi:http://dx.doi.org/10.1016/j.petrol.2006.03.026

Afidick, D., Kaczorowski, N. J., & Bette, S. (1994). *Production Performance of a Retrograde Gas Reservoir: A Case Study of the Arun Field*.

Ahmadi, M., Sharma, M. M., Pope, G., Torres, D. E., McCulley, C. A., & Linnemeyer, H. (2011). Chemical Treatment To Mitigate Condensate and Water Blocking in Gas Wells in Carbonate Reservoirs. doi:10.2118/133591-PA

Bang, V. S. S., Pope, G. A., Sharma, M. M., Baran, J. R., Jr., & Ahmadi, M. (2008). *A New Solution to Restore Productivity of Gas Wells with Condensate and Water Blocks*.

Barree, R. D., & Conway, M. W. (2004). *Beyond Beta Factors: A Complete Model for Darcy, Forchheimer, and Trans-Forchheimer Flow in Porous Media*.

Butler, M., Trueblood, J. B., Pope, G. A., Sharma, M. M., Baran, J. R., Jr., & Johnson, D. (2009). *A Field Demonstration of a New Chemical Stimulation Treatment for Fluid-Blocked Gas Wells*.

Craig, F. F. (1993). *The Reservoir Engineering Aspects Of Waterflooding* (Vol. 3): Society of Petroleum Engineers.

Dehane, A., & Tiab, D. (2000). *Performance of Horizontal Wells in Gas Condensate Reservoirs, Djebel Bissa Field, Algeria*.

Du, L., Walker, J. G., Pope, G. A., Sharma, M. M., & Wang, P. (2000). *Use of Solvents To Improve the Productivity of Gas Condensate Wells*.

Eikeland, K. M., & Hansen, H. (2009). Dry Gas Reinjection in a Strong Waterdrive Gas-Condensate Field Increases Condensate Recovery—Case Study: The Sleipner Øst Ty Field, South Viking Graben, Norwegian North Sea. doi:10.2118/110309-PA

Evans, E. V. (1994). *Dynamic Measurement of Sand-Pack Thickness and Evaluation of Non-Darcy Flow through Gravel-Packs.* (Doctor of Philosophy Dissertation), University of Oklahoma, Norman, Oklahoma.

Fahes, M. M., & Firoozabadi, A. (2007). Wettability Alteration to Intermediate Gas-Wetting in Gas-Condensate Reservoirs at High Temperatures. doi:10.2118/96184-PA

Fahimpour, J., Jamiolahmady, M., Severac, R., & Sohrabi, M. (2012). *Optimization of Fluorinated Wettability Modifiers for Gas-Condensate Carbonate Reservoirs*.

Kumar, V., Pope, G. A., & Sharma, M. M. (2006). *Improving the Gas and Condensate Relative Permeability Using Chemical Treatments*.

Li, K., & Firoozabadi, A. (2000). Experimental Study of Wettability Alteration to Preferential Gas-Wetting in Porous Media and Its Effects. doi:10.2118/62515-PA

Mousavi, M. A., Hassanajili, S., & Rahimpour, M. R. (2013). Synthesis of fluorinated nano-silica and its application in wettability alteration near-wellbore region in gas condensate reservoirs. *Applied Surface Science, 273*, 205-214. doi:http://dx.doi.org/10.1016/j.apsusc.2013.02.014

Pagliaro, M., & Ciriminna, R. (2005). New fluorinated functional materials. *Journal of Materials Chemistry, 15*(47), 4981-4991. doi:10.1039/B507583C

Panga, M. K. R., Ooi, Y. S., Koh, P. L., Chan, K. S., Enkababian, P. G., Cheneviere, P., & Samuel, M. M. (2006). *Wettability Alteration for Water Block Prevention in High Temperature Gas Wells*.

Sharifzadeh, S., Hassanajili, S., & Rahimpour, M. R. (2013). Wettability alteration of gas condensate reservoir rocks to gas wetness by sol–gel process using fluoroalkylsilane. *Journal of Applied Polymer Science, 128*(6), 4077-4085. doi:10.1002/app.38632

Tang, G.-Q., & Firoozabadi, A. (2002). Relative Permeability Modification in Gas/Liquid Systems Through Wettability Alteration to Intermediate Gas Wetting. doi:10.2118/81195-PA

Wu, S., & Firoozabadi, A. (2010). Effect of Salinity on Wettability Alteration to Intermediate Gas-Wetting. doi:10.2118/122486-PA

Zolotukhin, A. B., & Ursin, J. R. (1997). *Fundamentals of Petroleum Reservoir Engineering*. Norway: Høyskoleforlaget: Norwegian Academic Press.